Modeling minimum viable population size with multiple genetic problems of small populations

Peter NABUTANYI and Meike J. WITTMANN

Bielefeld University

Abstract

An important goal for conservation is to define minimum viable population (MVP) sizes for long-term persistence. Although many MVP size estimates focus on ecological processes, with increasing evidence for the role of genetic problems in population extinction, conservation practitioners have also increasingly started to incorporate the effects of deleterious mutations (DM) on fitness through inbreeding depression. However, small populations also face other genetic problems such as loss of genetic diversity through genetic drift that are usually factored into population viability assessments only via verbal arguments. A comprehensive quantitative theory on interacting genetic problems is missing. Here we develop eco-evolutionary quantitative models that track both population size and levels of genetic diversity. Our models assume a biallelic multilocus genome whose loci can be under either a single or interacting genetic forces. In addition to mutation-selection-drift balance (for loci under DM), we include three forms of balancing selection (for loci where variation is lost through genetic drift). We define MVP size as the lowest population size that avoids an eco-evolutionary extinction vortex. Our results show that MVP size decreases rapidly with increasing mutation rates for populations whose genomes are only under balancing selection, while for genomes under mutation-selection-drift balance, the MVP size increases rapidly. MVP sizes also increase rapidly with increasing number of loci under the same or different selection mechanisms until a point is reached at which even arbitrarily large populations cannot survive anymore. In the case of fixed number of loci under selection, interaction of genetic problems did not necessarily increase MVP sizes. To further enhance our understanding about interaction of genetic problems, there is need for more empirical studies to reveal how different genetic processes interact in the genome.

Introduction

In conservation management, the desire to protect threatened populations or species given limited available resources gave birth to the concept of a minimum viable population (MVP) size (Shaffer, 1981). Minimum viable population size is commonly defined as the lowest size that leads to population persistence for a specified duration with a set persistence probability, e.g., persistence for at least 1000 years with 99% probability or persistence for at least 50 generations with a probability of 90% (Shaffer, 1981; Traill et al., 2007). Alternatively, MVP size can be defined as the lowest size above which a substantial increase in extinction time occurs (Reed & Bryant, 2000) or in terms of fitness thresholds instead of persistence probability (Reed, 2005). So far, the choice of time and probability thresholds is arbitrary, varies among researchers, and across populations (Traill et al., 2007). This lack of consensus can make it hard to quantify relative extinction risk among different populations.

The viability of a small population and thus its MVP size depends on various ecological and genetic processes. Relevant ecological processes include demographic and environmental stochasticity, as well as Allee effects, e.g. through mate or pollen limitation at low density. In this study, however, we focus on the genetic processes shaping population viability and MVP sizes. In small populations, genetic problems such as effects of (partially) deleterious mutations (DM) and loss of genetic variation are inevitable (Lynch et al., 1995; Higgins & Lynch, 2001; Estes et al., 2004; Frankham, 2005; Coron et al., 2013). For example, increased homozygosity of deleterious alleles in small populations leads to a decrease in various fitness components, i.e. inbreeding depression (Spielman et al., 2004a; Bensch et al., 2006; Blomqvist et al., 2010; Palomares et al., 2012). Generally, genetic diversity is known to positively correlate with population size and influences population fitness (Reed & Frankham, 2003; Reed, 2005; Leimu et al., 2006; Hensen & Wesche, 2006; Kardos et al., 2021). For instance, over 70% of threatened species have lower heterozygosity than their taxonomically related non-threatened taxa (Spielman et al., 2004b). However, diversity at neutral marker loci and high population size are not always a good predictor of population fitness (Yates et al., 2019; Teixeira & Huber, 2021). Other factors such as the genetic architecture of fitness-relevant traits may have to be invoked for a better prediction of population fitness (Grossen et al., 2020; Kyriazis et al., 2021; Kardos & Luikart,

2021). But all in all, even if it is not always clear what aspects of diversity are most important and how they should be measured, there is increasing recognition for the importance of genetic diversity in population extinction (Frankham, 2005; Kardos et al., 2021).

To date, inbreeding depression is the only genetic problem of small population size that is routinely included in MVP studies, e.g. those that employ the software package *VORTEX* (Lacy, 1993). Thus, other genetic problems such as mutation accumulation and loss of genetic diversity through drift are ignored although they are known to be important contributors to extinction risk (Frankham, 2005). In nature, these problems may occur simultaneously in a small population. However, to the best of our knowledge, no studies exist that quantify the expected interaction of the different genetic problems. At best, the interaction is verbally projected to increase extinction risk.

Another key factor for long-term population persistence is how genetic diversity is maintained. It is now clear that both mutation-selection-drift equilibrium and balancing selection mechanisms maintain genetic variation in populations (e.g., Hughes & Nei, 1988; Gloss & Whiteman, 2016; Sharp & Agrawal, 2018), but balancing selection is still ignored in MVP studies. Balancing selection comes in various forms such as heterozygote advantage (HA), negative frequency-dependent selection (FD), and fluctuating selection with dominance reversals (FS), among others. The different forms of balancing selection can act in isolation or in some combination (e.g., Glémin et al., 2005; Hedrick, 2012; Bergland et al., 2014; Chen et al., 2015; Chapman et al., 2019; Mérot et al., 2020).

Our study has thus three goals: 1. to develop methods to account for genetic problems other than inbreeding depression in MVP studies, including loss of genetic variation at loci under balancing selection, 2. to quantify the effect of the interaction of two or more genetic problems on MVP sizes, and 3. to find ways to reduce the arbitrariness of time and persistence probability thresholds in MVP analyses. To this end, we developed eco-evolutionary models using three approaches, i.e., individual-based model, diffusion approximation, and equilibrium-based Markov chain approaches. We defined MVP size as the minimum population size that does not allow an eco-evolutionary extinction vortex to occur (with a certain probability) (Nabutanyi & Wittmann, 2021). An eco-evolutionary vortex occurs when the per-capita population growth rate turns negative. For the stochastic model, we used 95% persistence probability, but lower or higher probabilities did not substantially affect our

MVP size estimates. To reduce the arbitrariness of time thresholds used in most definitions of MVP size, in the Markov chain approach we used a long-term stable equilibrium perspective that does not require a time threshold.

General Model

Our models considered a diploid hermaphroditic population whose genome had multiple unlinked bi-allelic loci. The genome was acted on by either one selection mechanism at all loci or multiple mechanisms simultaneously, each at a set of loci. We developed three different approaches to quantifying minimum viable population size (Fig. 1).

The time-iterating approaches (one stochastic, one deterministic) considered populations initially at carrying capacity K with discrete-time population growth and non-overlapping generations. Here, the simulation tracked absolute fitness W and population size N until either the population went extinct or a set maximum number of generations (in this study, 1,000 generations) was reached. The MVP size was the lowest population size needed for at least 1 individual to survive at the end of the simulation. For the stochastic individual-based model (IBM), this condition had to be satisfied in at least 95% of the replicates. We also used a time-independent approach that assumed a population at equilibrium with a stationary distribution of allele frequencies and constant population size. Here we defined MVP size as the minimum size required for absolute fitness W at equilibrium to be at least 1.

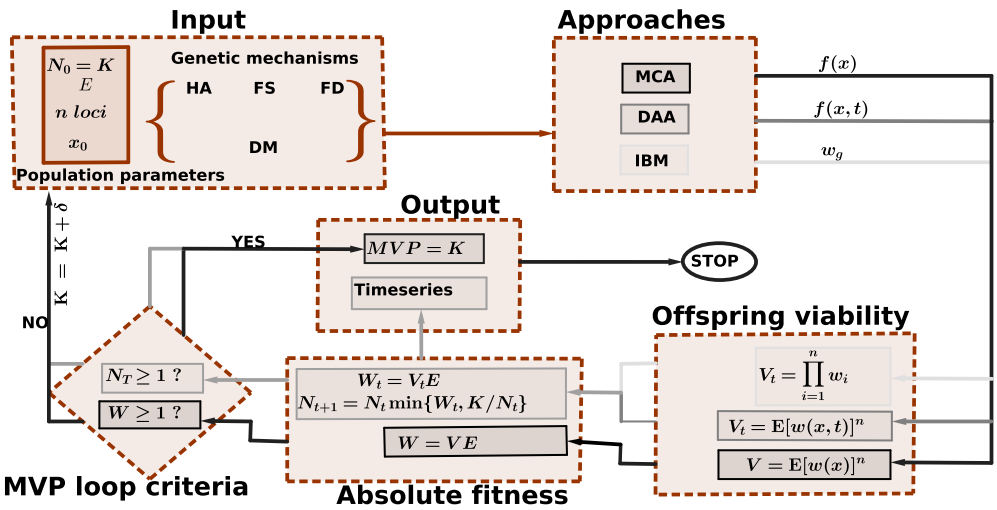

Figure 1: Overview of the three approaches to quantifying minimum viable population (MVP) sizes. For each population, we start with the required population parameters such as carrying capacity K, which also acts as the initial population size N_0, expected number of offspring E, the number of loci on the genome n, and initial allele frequency x_0. We then chose which selection mechanism(s) acts on the genome and simulated the population via either time-iterating approaches (i.e., diffusion approximation approach (DAA) or individual-based model (IBM)) or the equilibrium-based Markov chain approach (MCA). In the IBM, we tracked genotypes (and fitness) of each individual at each locus, and in DAA, we tracked allele frequency distribution $f(x,t)$ from which offspring viability V_t, absolute fitness W_t, and population size N_t were then sequentially determined. The iterations stopped when either the population went extinct or the maximum pre-set number of generations T was reached (whichever came first). In the MCA, we calculated the transition matrix for the number of allele copies at a constant population size from which the equilibrium allele-frequency distribution $f(x)$, viability V, and absolute fitness W, were sequentially determined. Starting with $K = 10$, we incremented K by δ in the MVP loop until either the MVP criterion was satisfied or set maximum value of K was reached (whichever came first).

Selection Mechanisms

We considered four selection scenarios: (partially) recessive deleterious mutations (DM) as well

as three forms of balancing selection i.e., heterozygote advantage (HA), fluctuating selection with dominance reversals (FS), and negative frequency-dependent selection (FD). For HA and DM, the relative fitnesses of the three genotypes AA, Aa, and aa at a given locus had the general form $w_{AA} = 1 - s_A, w_{Aa} = 1 - h \cdot s_a$, and $w_{aa} = 1 - s_a$, with the mechanisms differing in the magnitude of selection ($s_i; i = \{a, A\}$) and dominance (h) coefficients (Fig. 2a). In HA, $0 < s_A, s_a < 1$ and $h = 0$ such that the heterozygotes had higher relative fitness than either homozygote. For DM, $s_A = 0, 0 < s_a \leq 1$ and $0 \leq h \leq 1$. Thus, A was the wild-type allele and a the deleterious allele. Note that the DM scenario can model strongly recessive deleterious mutations of large effect which are the most important contributors to inbreeding depression, as well as more weakly deleterious mutations that can cause fitness deterioration via mutation accumulation.

For FS and FD, the relative fitnesses of genotypes fluctuated over time. In FS, the fluctuations depended on the temporal changes in selection coefficients (Fig. 2b and Appendix S1). With FD, the fluctuations depended on allele frequency whereby a genotype with a rarer allele was more fit. Thus, we set $w_{AA,t} = 1 - s_A x_t, w_{aa,t} = 1 - s_a(1 - x_t)$ and $w_{Aa,t} = 1 - \frac{x_t(s_A - s_a) + s_a}{2}$, where s_i was the maximum selection coefficient against the respective homozygote and x_t is the frequency of allele A at time t at a given locus.

For each selection mechanism above, we considered loci to be identical with respect to initial allele frequency, selection, and dominance coefficients, which greatly reduced simulation time in some approaches. However, in real populations, these parameters are usually not the same but have certain distributions, some of which are complex and vary across populations and species. Therefore, we also simulated populations were we drew selection coefficients s_a (and h), initial allele frequencies x_0, or both, from distributions (Table 1, Fig. 2b; see Section S2 for details). In the case of x_0, we sampled from a diffusion-based equilibrium allele frequency distribution . For balancing selection, $s_a = s_A$ at each locus. We also set $h = 0.5e^{-13s_a}$ for DM (Kardos et al., 2021), which accounts for the fact that more strongly deleterious mutations tend to be more recessive (Simmons & Crow, 1977; Eyre-Walker & Keightley, 2007; Agrawal & Whitlock, 2011).

Under balancing selection, the mutation rates were assumed to be symmetric, i.e., $\mu_A = \mu_a$, where μ_A and μ_a are the mutation rates from allele A to a and allele a to A respectively. For DM, we

assumed mutations from a to A to be rare and set $\mu_a = \frac{\mu_A}{100}$. We explored realistic ranges of mutation rates (in this study, $0 \leq \mu_A \leq 0.002$) (Tanaka, 1997; Estes et al., 2004) The number of loci were fixed during any simulation run. De novo mutations can be accounted for, but only to the extent that the fitness effects are the same as for a previous mutation that has been lost.

To understand the role of number of loci under selection and the interaction between different genetic mechanisms in the genome, we ran three types of simulation experiments. In the first type of experiment, genomes had $n = 100$ loci that were all under the same selection mechanism or evenly distributed between two, three or four mechanisms. In the second type of experiment, genomes had 1 to 1000 loci under a single selection mechanism. In the third type of experiment, genomes had 100 loci under one mechanism and 1 to 900 loci under a second mechanism. Note that these experiments were designed to give a qualitative understanding of interaction between loci and mechanisms for MVP sizes and that the numbers of loci may not necessarily represent realistic values for numbers of loci under selection in natural populations.

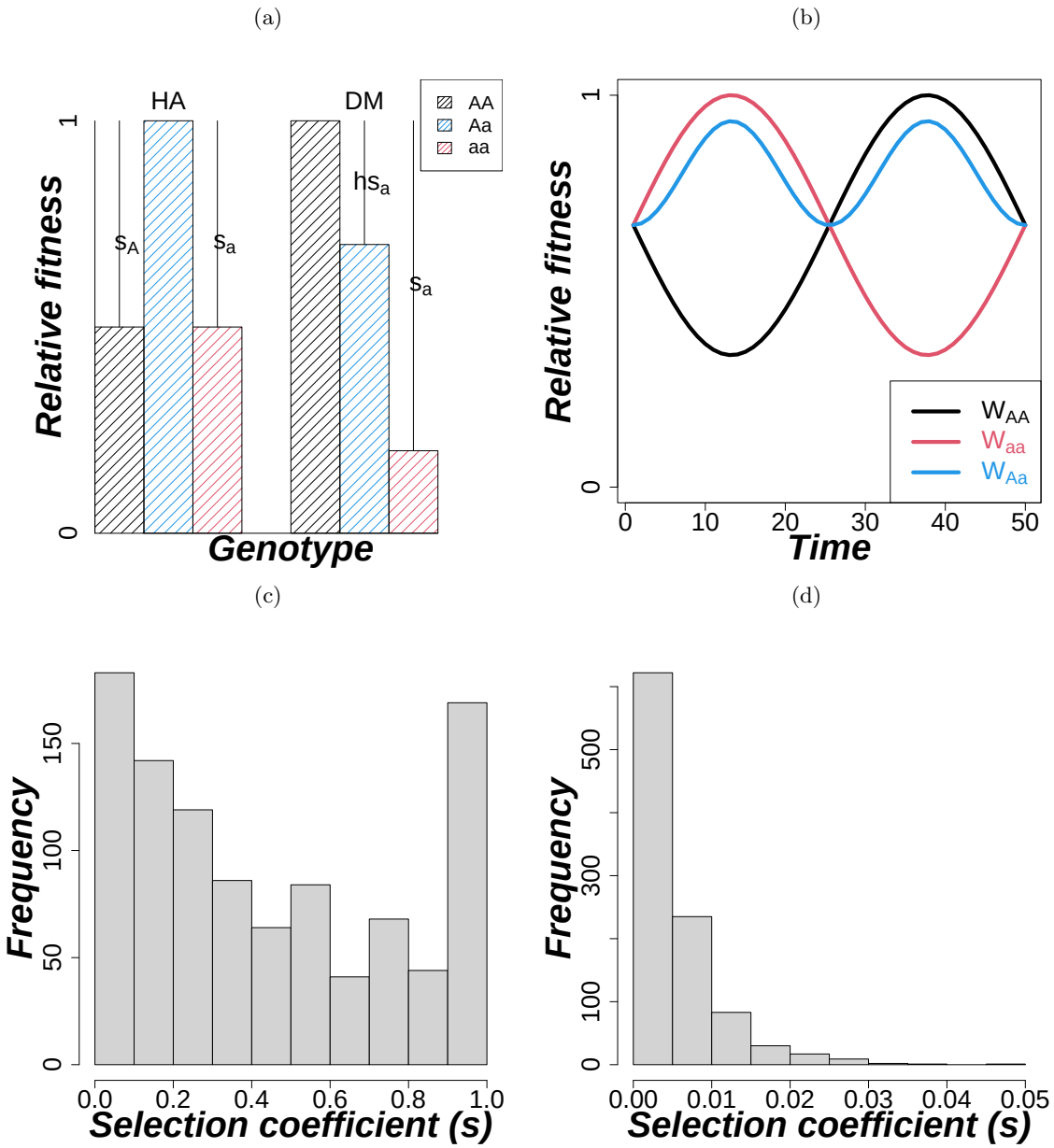

Figure 2: First row: Relative fitness of the genotypes under different selection mechanisms. (a) For heterozygote advantage (HA) and deleterious mutations (DM) whose relative fitness is constant through generations, and (b) for fluctuating selection with dominance reversals (FS), the relative fitness temporally fluctuates cyclically. We implemented this mechanism such that the heterozygote genotype is not the fittest in every generation but in any complete cycle of κ generations (we arbitrary used $\kappa = 50$), it emerged with a higher relative geometric mean fitness than either homozygote. Second row: Example distributions of selection coefficient s_a as obtained as described in Section S2 with mean parameter (c) $\overline{s} = 0.5$, (d) $\overline{s} = 0.005$. The former is a typical case of DM with large-effect mutations while the latter is a typical distribution for balancing selection scenarios as well as for DM with small-effect mutations.

Individual-Based Model (IBM) Simulations

The initial population size, N_0, was drawn from a Poisson distribution with mean K, the carrying capacity. For each individual and each locus, we then sampled 2 allele copies (with replacement) from the set $\{a, A\}$, where the probability to draw A was x_0.

In each generation, each parent produced a random number of offspring drawn from a Poisson distribution with mean E (1.53 in our default scenarios). The focal parent randomly chose a mating partner from all the available individuals including itself as a second parent for each offspring independently. For each locus, each partner independently and randomly passed on one of the available alleles to the respective offspring locus. Finally, the offspring alleles mutated with probability μ_A from A to a or μ_a from a to A.

Assuming multiplicative fitness across loci, each offspring was viable, i.e. survived, with probability, $V = \prod_{l=1}^{n} w_{g,l,t}$, where $w_{g,l,t}$ denotes the fitness of genotype $g \in \{AA,\ Aa,\ aa\}$ at locus l and generation t. After all individuals had reproduced, the surviving offspring replaced the parent generation. If there were more than K surviving offspring, only K offspring were randomly selected to replace the parents.

Deterministic Approximations to the Individual-Based Model

There were two main steps in the deterministic approximations, namely, approximating the distribution f_l of allele frequency x at locus l and determining the absolute fitness W using f_l. For the first step, f_l was determined by either the diffusion approximation approach (DAA) or the Markov chain approach (MCA).

The diffusion approximation involved numerically solving the diffusion equation

$$\frac{\partial f_l(x,t)}{\partial t} = -\frac{\partial \left[a_l(x,t) f_l(x,t)\right]}{\partial x} + \frac{1}{2}\frac{\partial^2 \left[b_l(x,t) f_l(x,t)\right]}{\partial x^2} \tag{1}$$

for $f_l(x,t)$ in each generation subject to some initial and boundary conditions (Zhao et al., 2013; Xu et al., 2019; Nabutanyi & Wittmann, 2021), where $a_l(x,t)$ and $b_l(x,t)$ are the mean and variance of the change in allele frequency during an infinitesimal time interval (Appendix S3.1). Here, $f_l(x,0)$

was a spike at x_0.

For the MCA, we assumed constant population size N and computed the transition probabilities of allele A from i copies at time t to j copies at time $t+1$ ($i, j \in \{0, 1, 2, \cdots, 2N\}$) for each locus separately. Assuming random sampling, the number of copies of the A allele in the next generation follows a binomial distribution with parameters $2N_t$ and x'' (the allele frequency after the action of selection and mutation). Due to numerical problems at large N ($N > 500$) with the binomial distribution, we approximated the transition probabilities using the Poisson distribution (when one of the alleles is rare) or the normal distribution (Appendix S3.2). Given the transition probability matrix, we then obtained the allele frequency distribution $f_l(x)$ as the eigenvector corresponding to the largest eigenvalue of the transition matrix. Appendix S3.2.1 also shows how MCA can be made time-dependent.

In the second step, we began by estimating the mean offspring viability V from $f_l(x)$. We let $n_{\mathcal{M}}$ be the number of loci under genetic mechanism $\mathcal{M}$. Then, assuming multiplicative fitness across loci and independence between loci, the fitness contribution from $\mathcal{M}$, is given by

$$V_{\mathcal{M}} = \prod_{l=1}^{n_{\mathcal{M}}} w_l(x_l), \tag{2}$$

where x_l is the allele frequency at the lth locus under mechanism $\mathcal{M}$ and the corresponding average fitness is

$$w_l(x_l) = x_l^2 w_{l,AA} + 2x_l(1-x_l)w_{l,Aa} + (1-x_l)w_{l,aa}. \tag{3}$$

Note that unlike in other parts of the text, here the index of x refers to the locus and not time.

Because the exact allele frequencies x_l are not explicitly known, we calculated $V_{\mathcal{M}}$ using the expected value of $w_l(x)$ under the equilibrium allele-frequency distribution f_l for the respective locus l

$$V_{\mathcal{M}} \approx \prod_{l=1}^{n_{\mathcal{M}}} \left(\sum_i f_l(b_i) w_l(b_i) \right), \tag{4}$$

where the sum is over all allele-frequency bins i. Also, assuming independence between selection

mechanisms, then, the offspring viability is $V = \prod_{\mathcal{M}} V_{\mathcal{M}}$.

The second step was completed by computing the absolute fitness, $W = VE$. Note that for DAA, the distribution f_l is calculated for every generation and so is $V_{\mathcal{M}}$ and W. Also, the population size N_{t+1} was determined from the previous generation t as

$$N_{t+1} = N_t \times \min\{W_t, \quad \frac{K}{N_t}\}. \tag{5}$$

Table 1: Parameters used in the main text under the different mechanisms. The values given are for the cases where genomes were treated to have identical loci. For cases where s_a and h was not uniform across loci, we sampled s_a from a distribution with each value sampled with a probability determined by an exponential distribution with mean $\overline{s} = s_a$. Also, for HA, FS, and FD, we set $s_a = s_A$ at each locus. See Section S2 for details on how the distributions for s_a were constructed. For time-iteration methods where x_0 was different across loci, we sampled the values for each locus independently from an equilibrium allele frequency distribution obtained via diffusion approximations (see Section S2).

Parameter	Description	HA	FS	FD	DM
s_a	Selection coefficient for allele a	0.005	0.005	0.005	0.5
s_A	Selection coefficient for allele A	s_a	s_a	s_a	0
h	Dominance coefficient for allele a				$0.5e^{-13s_a}$
μ_A	Mutation rate at each locus for allele A to a	$0 \leq \mu_a \leq 0.002$			
μ_a	Mutation rate at each locus for allele a to A	μ_A			$\frac{\mu_A}{100}$
x_0	Initial wild-type allele A frequency	0.5	0.5	0.5	0.95
κ	Number of generations in a complete cycle		50		
c	Used for determining dominance of the fitter allele		0.4		

Results

In this section, we focus on results from HA, FS, and DM. The results from FD are similar to those from HA (see supplementary Appendices S4 to S8).

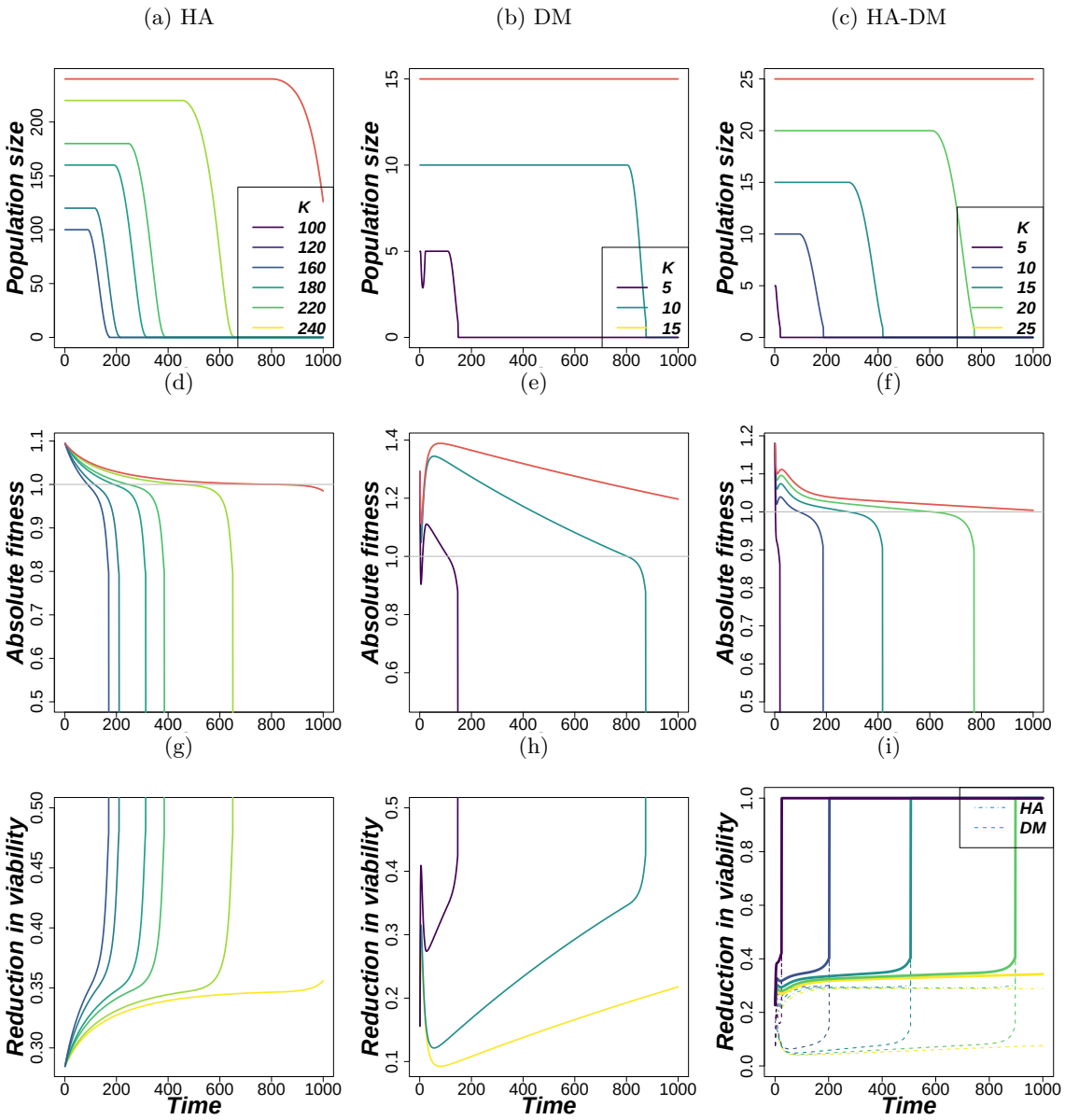

Figure 3: Example of typical trajectories under various carrying capacities with selection coefficients sampled from a distribution but uniform initial allele frequency across loci for; Column 1: HA, Column 2: DM, and Column 3: HA-DM, while for Row 1: population size, Row 2: absolute fitness, Row 3: reduction in viability fitness. The trajectories were obtained using the diffusion approximation approach (see Appendix S4.2 for some IBM trajectories). The gray horizontal line is the threshold absolute fitness of 1 while the red lines indicate the MVP size. The thick continuous lines on subfigure (i) is the net reduction in the viability fitness. Parameters were as described in Table 1 with $\mu_A = 0.0005$. Here, $h = 0.01$ for DM. The actual values of s_a for this figure are given in Section S2. Other shared parameters are $n = 100$. For scenarios with two selection mechanisms (column 3), 50 loci were under each mechanism. For population trajectories from other scenarios including those with uniform selection coefficients across loci, see Appendix S4.

Trajectories for population sizes and fitness obtained via the DAA approach are shown in Fig. 3. For both isolated and interacting selection mechanisms, the absolute fitness initially decreased while the population remained at the carrying capacity K (Fig. 3 rows 1 and 2, Appendices S4.1, S4.2). For relatively high K, absolute fitness decreased but stayed above 1, while populations remained at K. However, at lower K, absolute fitness decreased below a minimum threshold of 1 (gray line on Fig. 3 row 2). The populations started rapidly decreasing to extinction at the time when absolute fitness just fell below 1. However, under DM, there were some cases where an initial decline in absolute fitness below 1 caused no immediate rapid decline to extinction, probably as a result of purging deleterious mutations. The lowest carrying capacity that avoided population extinction was taken as the MVP size (indicated in red, Fig. 3 rows 1 and 2). The MVP size estimate from scenarios that involved DM increased with increasing simulation time (Appendix S4.1.1).

With interacting selection mechanisms, in the example in Fig. 3, the MVP size was intermediate between those for the isolated mechanisms, but on the same order of magnitude like the mechanism with the smaller MVP size (DM). The individual mechanisms reduced maximum offspring viability (which is 1) by different amounts that varied through time (Fig. 3, row 3). The rate at which locus fitness decreased (and attained equilibrium) also differed between constituent mechanisms. Generally, DM had a lower reduction in viability than balancing selection mechanisms in the earlier generations. However, the reduction in fitness due to DM eventually increased faster than that registered in the balancing selection mechanisms. Longer time series showed that DM takes relatively longer time to reach equilibrium (Section S4.1).

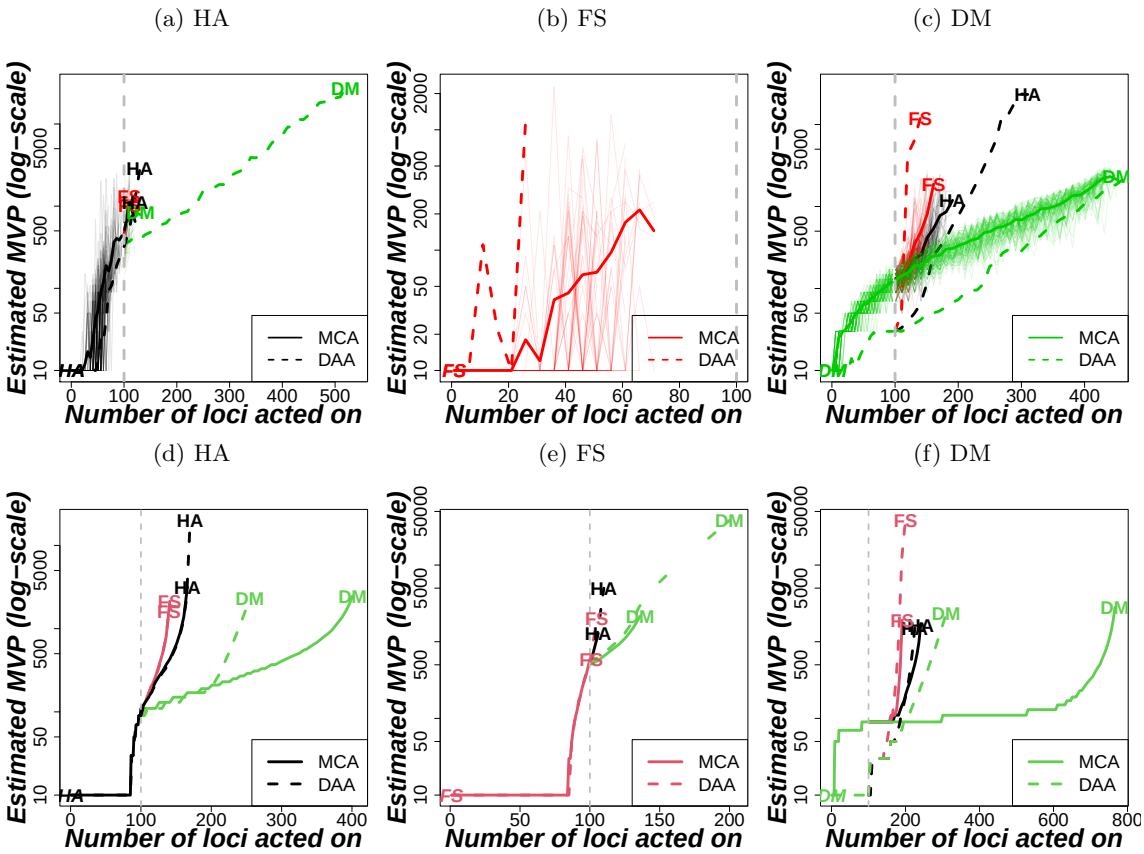

Figure 4:

Effect of increasing number of loci under selection on MVP size. (a) and (d) HA, (b) and (e) FS, and (c) and (f) DM. The first row selection coefficients across loci were picked from a distribution , whereas, the second row hasidentical loci under a given mechanism (same parameters). The genome from populations with at most 100 loci (below the vertical gray line) was acted on by the same selection mechanism (indicated at the start of the line). Those genomes with above 100 loci, the mechanism indicated at the end of the line acted on the remaining loci, e.g., the line with HA—DM label implies the first 100 loci were acted on by HA while DM acted on the remaining loci. In the first row, the thin lines are the 100 replicates obtained using MCA while the thick unbroken lines are the respective means of the 100 replicates and the broken thick line is the mean of 20 replicates from DAA. See Appendix S5.3 for results from more scenarios of parameter combinations, including cases where the initial allele frequency across loci is uniform for a given selection mechanism, but the selection coefficients are sampled. Parameters were as described in Table 1 with $\mu_A = 0.0005$.

In Fig. 4, we simulated different populations with different numbers of loci under selection using the DAA and MCA approaches. The MVP size initially remained constant at 10 (our lowest tested population size) as the number of loci increased until a certain number was reached where a rapid increase was registered. Even under the same selection mechanism, the rate at which log MVP size increased decreased after a certain number of loci. As more loci were added, log MVP size again increased rapidly, producing an inflection point (Fig. 4 row 2). Note though that on a linear scale, MVP size increases more and more rapidly with increasing number of loci and there is no inflection point, except for DM which according to the MCA mechanism still exhibits an inflection point (Appendix S5.3), which could be because of a different shape of viability as a function of population size (Appendix S7). At a certain critical number of loci, MVP sizes exhibited an asymptotic increase (to infinity), indicating that no finite population size was sufficient to keep the population at equilibrium. Note that in cases of uniform parameters across loci, we tested K values from 10 to 150000 using DAA (10 to 3500 using MCA) and numbers of loci from 1 to 1000 for all the scenarios. Unlike for DM, for balancing selection mechanisms the critical number of loci required for an asymptotic increase in MVP size was independent of mutation rates (Appendices S5 and S5.3). Also, MCA produced higher MVP estimates than DAA in some cases of DM scenarios, but the divergence disappeared as more loci were added.

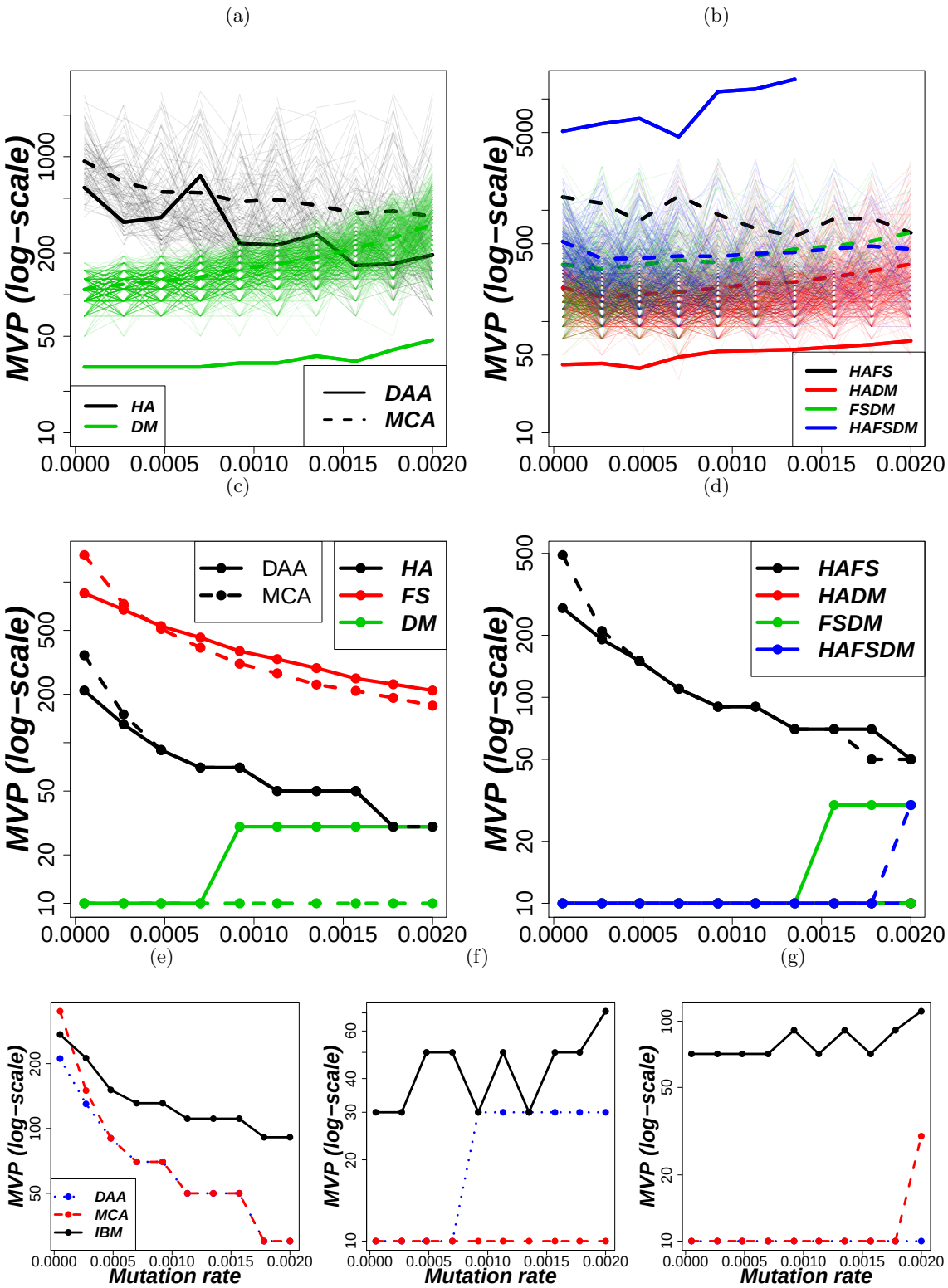

Figure 5: Variation of MVP size with mutation rate μ_A. 1st row: Both selection coefficients (s_a) and initial allele frequencies (x_0) sampled from distributions. The thin lines are the 100 MCA replicates while the thick broken lines are the respective replicate means and the unbroken thick lines are the mean of 20 DAA replicates. 2nd and 3rd rows: Identical loci (same s_a and x_0) under a mechanism with (e) HA only, (f) DM only and (g) HA-FS-DM. Number of IBM replicates = 20. $n = 100$ except for combinations with 3 mechanisms where $n = 99$ for purposes of equal distribution of loci. See Table 1 for other parameter description.

The effect of mutation rate on MVP sizes varied strongly among genetic mechanisms (Fig. 5). For genomes that were acted on by only balancing selection mechanisms either separately or simultaneously, the MVP size estimates generally decreased rapidly with mutation rates. By contrast, MVP estimates under DM increased rapidly.

With a fixed total number of loci under selection, in genomes with more than one mechanism, the joint MVP size was in most cases closer to the harmonic (or geometric) mean of the MVP estimates obtained when the constituent selection mechanisms acted in isolation than to the arithmetic mean (Appendix S6.3). However, there were also exceptions where the joint MVP size was close to or even larger than the arithmetic mean of single MVP sizes.

In most scenarios that contained only balancing selection, the estimates from DAA and MCA roughly coincided, but for DM there were quantitative differences between DAA and MCA approach (Fig. 5 rows 1 and 2). Sampling s_a and/or x_0 from distributions produced higher MVP size estimates than with fixed values across loci, producing some qualitative effects in some cases. For example, DAA produced lower estimates than MCA for DM s_a and x_0 are sampled and vice versa for identical loci under a given mechanism (comparing rows 1 and 2 on Fig. 4, 5). The IBM estimates were more variable (possibly because of fewer number of replicates) and were (slightly) higher than estimates from DAA, and converged better to the MCA and DAA estimates at higher MVP sizes (Fig. 5 row 3). Also, the IBM estimates were fairly insensitive to levels of survival probability thresholds (Appendix S6.1).

Discussion

Small populations can be faced with multiple genetic problems simultaneously. In this study, we quantified the effect of such interactions on extinction risk by estimating MVP sizes. MVP size rapidly increased as more loci under selection were added. However, when the total number of loci in the genome was fixed, MVP size estimates were in most but not all of the scenarios we considered dominated by the mechanism that yielded the lowest estimate when acting alone on the genome.

Number of loci under selection

As the number of loci under selection increased, cumulative selection pressure on the genome increased and as a result, offspring viability decreased, thus increasing MVP size. Under balancing selection mechanisms, the critical number of loci above which no arbitrary population size survived was independent of mutation rates and decreased with increasing selection coefficients (Appendix S5). This is because, in an infinite population under symmetric balancing selection and symmetric mutation rates, equilibrium fitness is independent of mutation rates. Moreover, heterozygosity increases with increasing mutation rate, which increases population fitness. Thus MVP estimates are lower at higher mutation rates. By contrast, the critical number of loci under mutation-selection-balance was independent of the selection coefficient but decreased with an increase in mutation rates. This is in agreement with classical studies showing that equilibrium fitness only depends on mutation rate (μ_A) and not on selection coefficient (s_a) if $\mu_A << s_a$ (Haldane, 1937; Agrawal & Whitlock, 2012; Felsenstein, 2015).

Most of the predominance of the mechanism that yielded the lowest MVP estimate in the fixed number of loci scenario can be explained by the relationship between viability per locus and population size. In Appendix S7, we assume that viability increases linearly with population size with a common intercept, and show that the joint MVP is approximately equal to the harmonic mean of the MVPs obtained from the constituent mechanisms when acting in isolation. We also illustrate scenarios where the joint MVP can be even higher than the harmonic, geometric, and arithmetic means as also observed in some cases in our results.

DAA, MCA, and IBM

In many regions of parameter space, the three approaches largely agreed in their MVP size estimates qualitatively and quantitatively, but there were also discrepancies and each approach has its advantages and disadvantages. For example, the relatively low MVP estimates from the iterating approaches in DM at low mutation rates can be attributed to lack of attainment of a stationary allele frequency distribution within the simulated period of time. For example, for mutation rate of $\mu_A = 0.00005$ and $\mu_a = \frac{\mu_A}{100}$, equilibrium is attained only after at least $\frac{1}{\mu_A+\mu_a} \approx 20,000$ generations

from mutation alone (see Felsenstein, 2015). The equilibrium-based MCA estimates did not depend on the length of the simulation period and the initial conditions. Therefore, MCA estimates can be considered as the "true" MVP estimates if one is interested in the possibility of a long-term stable population. However, MCA may give overly optimistic predictions for population survival if the population considered starts far from genetic equilibrium (Appendix S8; see also Kardos & Luikart, 2021). For example, during founder events, population fragmentation, and bottlenecks, deleterious allele frequencies may be above equilibrium values such that populations may be unable to replace themselves in the early generations and go extinct before reaching a genetic equilibrium. The time-dependent approaches could account for such transient dynamics, but for this the initial genetic composition of the population needs to be known. Sampling initial allele frequencies x_0 from the equilibrium allele frequency distribution yields higher MVP estimates because, at relatively lower population sizes. For balancing selection, in small population sizes at equilibrium extreme allele frequencies close to 0 and 1 are more likely. With symmetric selection, the high proportion of homozygotes in the initial populations are less fit and population sizes are more likely to decrease rapidly to extinctions in the earlier generations requiring relatively higher sizes for initial survival. Similarly, under DM, sampling x_0 resulted in higher number of lethal equivalents in smaller initial populations than larger ones. Generally number of lethal equivalents ranged between 2 (with 100 loci and $\overline{s} = 0.5$) to 40 (with 1000 loci and $\overline{s} = 0.5$) (see some trajectories of lethal equivalents in Section S4.1). These values are in the range of empirically estimated numbers of lethal equivalents in natural populations (Ralls et al., 1988; O'Grady et al., 2006).

Unlike in the DAA and MCA approaches where allele frequencies evolve completely independently across loci, in the IBM evolution at one locus can potentially interfere with evolution at another locus, making the fitnesses of the genotypes at the focal locus more variable. IBMs also have the advantage that they take into account demographic stochasticity (which in some cases led to higher MVP size estimates than for the MCA and DAA approach). Therefore IBM gives a better representation of natural populations. However, IBMs are extremely time-consuming especially at higher carrying capacity since many replicates are required to infer MVP sizes. Similarly, obtaining the transition matrix in the MCA is computationally impossible for higher carrying capacity. On the other hand, the accuracy in DAA depends the discretization of allele frequency, x and can perform

poorly for very small population sizes. Thus each of the approaches will be most useful in a different context: MCA to get long-term predictions for small populations, IBM for small populations when demographic stochasticity and inter-locus interactions should be accounted for, and DAA for large populations.

Choice of the MVP Definition Thresholds

In the case of more than one threatened population, managers may have to prioritise allocation of available limited resources. Therefore, there is need to establish relative viability status of the populations, e.g. by comparing required MVP sizes to current population sizes. Equilibrium-based MVP sizes could help make MVP sizes more comparable across populations, while still taking into account specific population parameters. In the IBM, our estimates were largely insensitive to survival thresholds (Appendix S6.1), possibly due to relatively low stochasticity in the model. We expect survival thresholds to be more important when environmental stochasticity is included.

Furthermore, we chose an extinction threshold of 1 individual for the time-iterating approaches. However, larger thresholds could also be chosen for dioecious populations and populations that suffer from Allee effects due to mate-finding difficulties or other ecological problems at low population size. For the MCA with equilibrium assumptions, a quasi-extinction threshold of absolute fitness 1 was used. The absolute fitness of 1 acts as a boundary between population persistence ($W > 1$) and population decline ($W < 1$) in an eco-evolutionary extinction vortex (Nabutanyi & Wittmann, 2021).

Concluding Remarks and Recommendations

Given that many of the parameters of our model are chosen somewhat arbitrarily (as well as in many other studies) and cannot be estimated precisely and that we did not take into account factors like environmental stochasticity that are also important for extinction risk, the numbers we obtain as MVP sizes should not be interpreted too literally, but rather relative to each other as measures of relative extinction risk. Also, since our models assumed an idealized randomly mating population with a long-term viability perspective, the estimates in this paper should be compared to the genetically derived effective population sizes in the literature such as the long-term 500 estimate in the 50/500 rule of thumb (Franklin, 1980; Frankham et al., 2014).

To promote a qualitative understanding of the interaction of different genetic mechanisms, we have also simulated simplified scenarios where each genetic mechanism affects the same number of loci. In nature, this is unlikely to be the case. In fact, the relative contribution of mutation-selection-drift balance, positively selected mutations on their way to fixation, and the various forms of balancing selection (heterozygote advantage, negative frequency-dependent selection, heterogeneous selection in space or time), to overall genetic and phenotypic variation is one of the most important but still largely open questions in evolutionary biology (Mitchell-Olds et al., 2007). In one of the few studies putting numbers to the respective contributions, Sharp & Agrawal (2018) estimated (after correcting for two sources of bias) that in *Drosophila melanogaster* 12 % of variation in male mating success, 33 % of variation in female fecundity, and 86 % of variation in larval viability can be explained by mutation-selection balance, with the rest potentially being due to various forms of balancing selection. Other studies have similarly found that mutation-selection balance is insufficient to explain observed patterns of variation (Kelly & Willis, 2001; Charlesworth et al., 2007; Charlesworth, 2015). However, at the moment it is unclear how robust these numbers are and whether they transfer to other species. Thus the current state of knowledge is not good enough to parameterize a model such as ours with realistic proportions of loci under each mechanism. Nevertheless, it is becoming clear that balancing selection in its various forms may be more common in natural populations than earlier proclaimed (Chapman et al., 2019; Mérot et al., 2020). Thus we suggest that it would make sense to incorporate balancing selection mechanisms into software tools designed to evaluate population persistence. Furthermore, our observations were based on independence between loci. Epistasis and linkage disequilibrium may give different results. Therefore, to improve extinction risk assessment, a better understanding of the underlying genetic processes in a given population is needed.

To better understand how interacting genetic problems affect population persistence, empirical studies are needed. There are many technical challenges in obtaining the necessary detailed genetic information, e.g., identifying which and how many loci are responsible for specific fitness traits, and which genetic mechanism(s) maintain variation at which loci. However, current studies are already heading in the right direction. For example, laboratory experiments with *Drosophila melonagaster* can now distinguish the contributions of different genetic mechanisms in maintaining variation at a given locus (Charlesworth, 2015; Sharp & Agrawal, 2018). In addition, modern sequencing tech-

niques can allow quantitative trait loci to be mapped to different fitness components and genomic regions with traits that influence fitness components (such as survival and fecundity) can be identified from neutral quantitative trait loci (Ågren et al., 2013). Note though that identifying all relevant loci, even those with small effect, is not feasible for model organisms, and much less for threatened populations.

To conclude, our results revealed that if the number of loci under selection is fixed, a mixture of genetic processes is not necessarily worse than having the same genetic mechanism acting at all loci. However, if the total number of loci under selection increases, for example because genetic mechanisms that were previously neglected are now included, estimated extinction risk and MVP sizes can dramatically increase. These observations call for inclusion of all genetic processes in assessing the viability of populations. Populations normally also face other ecological problems such as environmental stochasticity and Allee effects, and their consideration is expected to further increase extinction risk and MVP size estimates (Tanaka, 2000; Wittmann et al., 2018).

Supporting Information

In the supplementary material, we briefly show the mathematical derivation for FS (Appendix S1). In Appendix S3, we provide more details about DAA and MCA. Appendices S4 through S8 provide some additional results that also involve FD. Also, we show how estimates of minimum viable population size depend on fitness per locus (Appendix S7) and how equilibrium fitness and critical number of loci can be estimated (Appendix S5).

References

Agrawal, A.F. & Whitlock, M.C. (2011) Inferences about the distribution of dominance drawn from yeast gene knockout data. *Genetics* 187, 553–566.

Agrawal, A.F. & Whitlock, M.C. (2012) Mutation load: the fitness of individuals in populations where deleterious alleles are abundant. *Annual Review of Ecology, Evolution, and Systematics* 43, 115–135.

Ågren, J., Oakley, C.G., McKay, J.K., Lovell, J.T. & Schemske, D.W. (2013) Genetic mapping of adaptation reveals fitness tradeoffs in *Arabidopsis thaliana*. *Proceedings of the National Academy of Sciences* 110, 21077–21082.

Bensch, S., Andrén, H., Hansson, B., Pedersen, H.C., Sand, H., Sejberg, D., Wabakken, P., Åkesson, M. & Liberg, O. (2006) Selection for heterozygosity gives hope to a wild population of inbred wolves. *PloS One* 1, e72.

Bergland, A.O., Behrman, E.L., O'Brien, K.R., Schmidt, P.S. & Petrov, D.A. (2014) Genomic evidence of rapid and stable adaptive oscillations over seasonal time scales in *Drosophila*. *PLoS Genetics* 10, e1004775.

Blomqvist, D., Pauliny, A., Larsson, M. & Flodin, L.Å. (2010) Trapped in the extinction vortex? Strong genetic effects in a declining vertebrate population. *BMC Evolutionary Biology* 10, 33.

Chapman, J.R., Hill, T. & Unckless, R.L. (2019) Balancing selection drives the maintenance of genetic variation in *Drosophila* antimicrobial peptides. *Genome biology and evolution* 11, 2691–2701.

Charlesworth, B. (2015) Causes of natural variation in fitness: evidence from studies of *Drosophila* populations. *Proceedings of the National Academy of Sciences* 112, 1662–1669.

Charlesworth, B., Miyo, T. & Borthwick, H. (2007) Selection responses of means and inbreeding depression for female fecundity in drosophila melanogaster suggest contributions from intermediate-frequency alleles to quantitative trait variation. *Genetics Research* 89, 85–91.

Chen, J., Nolte, V. & Schlötterer, C. (2015) Temperature stress mediates decanalization and dominance of gene expression in *Drosophila melanogaster*. *PLoS Genetics* 11, e1004883.

Coron, C., Méléard, S., Porcher, E. & Robert, A. (2013) Quantifying the mutational meltdown in diploid populations. *The American Naturalist* 181, 623–636.

Durrett, R. (2008) *Probability models for DNA sequence evolution*. Springer-Verlag, Ithaca, New York.

Estes, S., Phillips, P.C., Denver, D.R., Thomas, W.K. & Lynch, M. (2004) Mutation accumulation in populations of varying size: the distribution of mutational effects for fitness correlates in *Caenorhabditis elegans*. *Genetics* 166, 1269–1279.

Eyre-Walker, A. & Keightley, P.D. (2007) The distribution of fitness effects of new mutations. *Nature Reviews Genetics* 8, 610–618.

Felsenstein, J. (2015) Theoretical evolutionary genetics, genome 562. *University of Washington, Seattle, Washington* pp. 135–155.

Frankham, R. (2005) Genetics and extinction. *Biological Conservation* 126, 131–140.

Frankham, R., Bradshaw, C.J. & Brook, B.W. (2014) Genetics in conservation management: revised recommendations for the 50/500 rules, red list criteria and population viability analyses. *Biological Conservation* 170, 56–63.

Franklin, I.R. (1980) Evolutionary changes in small populations. *In: Michael E. Soulé and B. M. Wilcox, Eds., Conservation Biology: An Evolutionary-Ecological Perspective* pp. 135–149.

Glémin, S., Gaude, T., Guillemin, M.L., Lourmas, M., Olivieri, I. & Mignot, A. (2005) Balancing selection in the wild: testing population genetics theory of self-incompatibility in the rare species *Brassica insularis*. *Genetics* 171, 279–289.

Gloss, A.D. & Whiteman, N.K. (2016) Balancing selection: Walking a tightrope. *Current Biology* 26, R73–R76.

Grossen, C., Guillaume, F., Keller, L.F. & Croll, D. (2020) Purging of highly deleterious mutations through severe bottlenecks in Alpine ibex. *Nature communications* 11, 1–12.

Haldane, J. (1937) The effect of variation of fitness. *The American Naturalist* 71, 337–349.

Hedrick, P.W. (2012) What is the evidence for heterozygote advantage selection? *Trends in Ecology & Evolution* 27, 698–704.

Hensen, I. & Wesche, K. (2006) Relationships between population size, genetic diversity and fitness components in the rare plant *Dictamnus albus* in Central Germany. *Biodiversity and Conservation* 15, 2249–2261.

Higgins, K. & Lynch, M. (2001) Metapopulation extinction caused by mutation accumulation. *Proceedings of the National Academy of Sciences* 98, 2928–2933.

Hughes, A.L. & Nei, M. (1988) Pattern of nucleotide substitution at major histocompatibility complex class I loci reveals overdominant selection. *Nature* 335, 167–170.

Kardos, M., Armstrong, E., Fitzpatrick, S., Hauser, S., Hedrick, P., Miller, J., Tallmon, D.A. & Funk, W.C. (2021) The crucial role of genome-wide genetic variation in conservation. *bioRxiv* .

Kardos, M. & Luikart, G. (2021) The genetic architecture of fitness drives population viability during rapid environmental change. *The American Naturalist* 197, 511–525.

Kelly, J.K. & Willis, J.H. (2001) Deleterious mutations and genetic variation for flower size in *Mimulus guttatus*. *Evolution* 55, 937–942.

Kimura, M. et al. (1955) Stochastic processes and distribution of gene frequencies under natural selection. *Cold Spring Harbor Symposia on Quantitative Biology* 20, 33–53.

Kyriazis, C.C., Wayne, R.K. & Lohmueller, K.E. (2021) Strongly deleterious mutations are a primary determinant of extinction risk due to inbreeding depression. *Evolution Letters* 5, 33–47.

Lacy, R.C. (1993) VORTEX - a computer simulation model for population viability analysis. *Wildlife Research* 20, 45–65.

Leimu, R., Mutikainen, P., Koricheva, J. & Fischer, M. (2006) How general are positive relationships between plant population size, fitness and genetic variation? *Journal of Ecology* 94, 942–952.

Lynch, M., Conery, J. & Burger, R. (1995) Mutation accumulation and the extinction of small populations. *The American Naturalist* 146, 489–518.

Mérot, C., Llaurens, V., Normandeau, E., Bernatchez, L. & Wellenreuther, M. (2020) Balancing selection via life-history trade-offs maintains an inversion polymorphism in a seaweed fly. *Nature communications* 11, 1–11.

Mitchell-Olds, T., Willis, J.H. & Goldstein, D.B. (2007) Which evolutionary processes influence natural genetic variation for phenotypic traits? *Nature Reviews Genetics* 8, 845–856.

Nabutanyi, P. & Wittmann, M.J. (2021) Models for eco-evolutionary extinction vortices under balancing selection. *The American Naturalist* 197, 336–350.

O'Grady, J.J., Brook, B.W., Reed, D.H., Ballou, J.D., Tonkyn, D.W. & Frankham, R. (2006) Realistic levels of inbreeding depression strongly affect extinction risk in wild populations. *Biol. Conserv.* 133, 42–51.

Palomares, F., Godoy, J.A., López-Bao, J.V., RodrÍguez, A., Roques, S., Casas-Marce, M., Revilla, E. & Delibes, M. (2012) Possible extinction vortex for a population of Iberian lynx on the verge of extirpation. *Conservation Biology* 26, 689–697.

Ralls, K., Ballou, J.D. & Templeton, A. (1988) Estimates of lethal equivalents and the cost of inbreeding in mammals. *Conservation biology* 2, 185–193.

Reed, D.H. (2005) Relationship between population size and fitness. *Conservation biology* 19, 563–568.

Reed, D.H. & Bryant, E.H. (2000) Experimental tests of minimum viable population size. *Animal Conservation* 3, 7–14.

Reed, D.H. & Frankham, R. (2003) Correlation between fitness and genetic diversity. *Conservation Biology* 17, 230–237.

Shaffer, M.L. (1981) Minimum population sizes for species conservation. *BioScience* 31, 131–134.

Sharp, N.P. & Agrawal, A.F. (2018) An experimental test of the mutation-selection balance model for the maintenance of genetic variance in fitness components. *Proceedings of the Royal Society B* 285, 20181864.

Simmons, M.J. & Crow, J.F. (1977) Mutations affecting fitness in drosophila populations. *Annual Review of Genetics* 11, 49–78.

Spielman, D., Brook, B.W., Briscoe, D.A. & Frankham, R. (2004a) Does inbreeding and loss of genetic diversity decrease disease resistance? *Conservation Genetics* 5, 439–448.

Spielman, D., Brook, B.W. & Frankham, R. (2004b) Most species are not driven to extinction before genetic factors impact them. *Proceedings of the National Academy of Sciences* 101, 15261–15264.

Tanaka, Y. (1997) Extinction of populations due to inbreeding depression with demographic disturbances. *Researches on Population Ecology* 39, 57–66.

Tanaka, Y. (2000) Extinction of populations by inbreeding depression under stochastic environments. *Population Ecology* 42, 55–62.

Teixeira, J.C. & Huber, C.D. (2021) The inflated significance of neutral genetic diversity in conservation genetics. *Proceedings of the National Academy of Sciences* 118, e2015096118.

Traill, L.W., Bradshaw, C.J. & Brook, B.W. (2007) Minimum viable population size: a meta-analysis of 30 years of published estimates. *Biological conservation* 139, 159–166.

Wittmann, M.J., Stuis, H. & Metzler, D. (2018) Genetic Allee effects and their interaction with ecological Allee effects. *Journal of Animal Ecology* 87, 11–23.

Xu, S., Chen, M., Liu, C., Zhang, R. & Yue, X. (2019) Behavior of different numerical schemes for random genetic drift. *BIT Numerical Mathematics* pp. 1–25.

Yates, M., Bowles, E. & Fraser, D. (2019) Small population size and low genomic diversity have no effect on fitness in experimental translocations of a wild fish. *Proceedings of the Royal Society B* 286, 20191989.

Zhao, L., Yue, X. & Waxman, D. (2013) Complete numerical solution of the diffusion equation of random genetic drift. *Genetics* 194, 973–985.

Appendices

S1 Brief Description of Fluctuating Selection with Reversal of Dominance (FS)

Briefly, FS was derived as follows (see Nabutanyi & Wittmann (2021) for a detailed description). The relative fitnesses of the genotypes were $w_{AA,t} = (1 - s_{A,t})/\mathcal{C}$, $w_{aa,t} = (1 - s_{a,t})/\mathcal{C}$ and $w_{Aa,t} = (1 - h_t \cdot s_{A,t} - (1 - h_t) \cdot s_{a,t})/\mathcal{C}$, where $s_{A,t} = s_A \cdot \sin(2\pi \cdot t/\kappa)$ and $s_{a,t} = s_a \cdot \sin(\pi + 2\pi \cdot t/\kappa)$ are temporally fluctuating selection coefficients and $h_t = 0.5 - c \cdot \sin(2\pi \cdot t/\kappa)$ is the temporally fluctuating dominance coefficient. Here, $\mathcal{C} = 1 + \max(s_a, s_A)$ is the normalization constant such that the genotype fitness lies between 0 and 1, s_A and s_a determine the amplitude of selection and $0 \leq c \leq 0.5$ determines the strength of dominance. We arbitrarily used $c = 0.4$ and $\kappa = 50$ throughout the paper, where κ is the number of generations in a complete cycle.

S2 Selection Coefficient and Initial Allele Frequency Distributions

We first modelled all the loci as identical i.e., with same initial allele frequency, selection, and dominance coefficients. This greatly simplified the mathematical simulations and saved simulation time in some approaches. However, in real populations, these parameters are usually not the same but have certain distribution, some of which are complex and vary across populations and species (Eyre-Walker & Keightley, 2007; Agrawal & Whitlock, 2011). Thus we also simulated populations with a distribution of either selection coefficients, initial allele frequencies, or both.

First, we constructed the sample space for selection coefficients $s = 20^y$ between 0 and 1, where y represents a total of 15 values that are evenly spaced on the interval $-1.9 \leq y \leq -0.001$ (Table S2.1, left column). The cumulative distribution function (CDF) of s was obtained using an exponential

distribution with mean $\overline{s}$.

The actual probability of each value of s was then determined by getting the probability of each bin of the distribution (here, each bin contained exactly only one value of s and the difference between consecutive CDF points taken as the probability of the respective value, i.e., the first value takes the first value of the CDF and the corresponding values assigned the respective differences between points of the CDF). In cases where the total probability was less than 1, the probability of the last bin was added the difference. This is similar to randomly picking 15 values from an exponential distribution with mean $\overline{s}$ but coercing all values above 1 (our feasible maximum for s) to 1.

During the simulation, for each locus, the value of s_a was sampled from an s distribution with mean $\overline{s}$. For balancing selection, we set $s_A = s_a$. For deleterious mutations (DM), $h = 0.5e^{-13s_a}$. To allow a fair comparison with cases where loci had uniform selection coefficients, the value of s_a in the uniform loci cases were set to $\overline{s}$.

Table S2.1: Distribution of selection coefficients, s_a for the trajectories in Figure 3 in the main text. HA_1 for the 1st column, DM_2 for the second column, HA_3 for the 50% of loci in the 3rd column, and DM_3 for the 50% of loci in the 3rd column in Figure 3.

s_a	HA_1	DM_2	HA_3	DM_3
0.00337	50	0	23	0
0.00506	14	0	7	0
0.00760	14	1	9	0
0.01141	11	0	3	0
0.01714	10	0	7	1
0.02573	1	1	1	0
0.03863	0	0	0	1
0.05799	0	2	0	4
0.08707	0	6	0	1
0.13071	0	8	0	5
0.19624	0	12	0	3
0.29463	0	14	0	5
0.44233	0	10	0	9
0.66408	0	14	0	12
0.99701	0	32	0	9

In addition to simulating populations with same initial allele frequency, x_0, across loci for a given mechanism for the IBM and DAA, we simulated populations where x_0 was sampled for each locus from an equilibrium distribution $\phi(x)$ based on a diffusion approximation (see e.g., Durrett, 2008;

Felsenstein, 2015)

$$\phi(x) = x^{4N_e\mu_a - 1}(1-x)^{4N_e\mu_A - 1}V^{2N_e}, \tag{S2.1}$$

where x is the allele frequency, N_e is the effective population size (here $N_e = K$), and V is the population mean fitness which is a function of x, s_a, s_A and h. In cases where $V^{2N_e} = 0$ due to either large s_a, s_A or N_e, we set $x_0 = 0.5$ for balancing selection (DM was not affected).

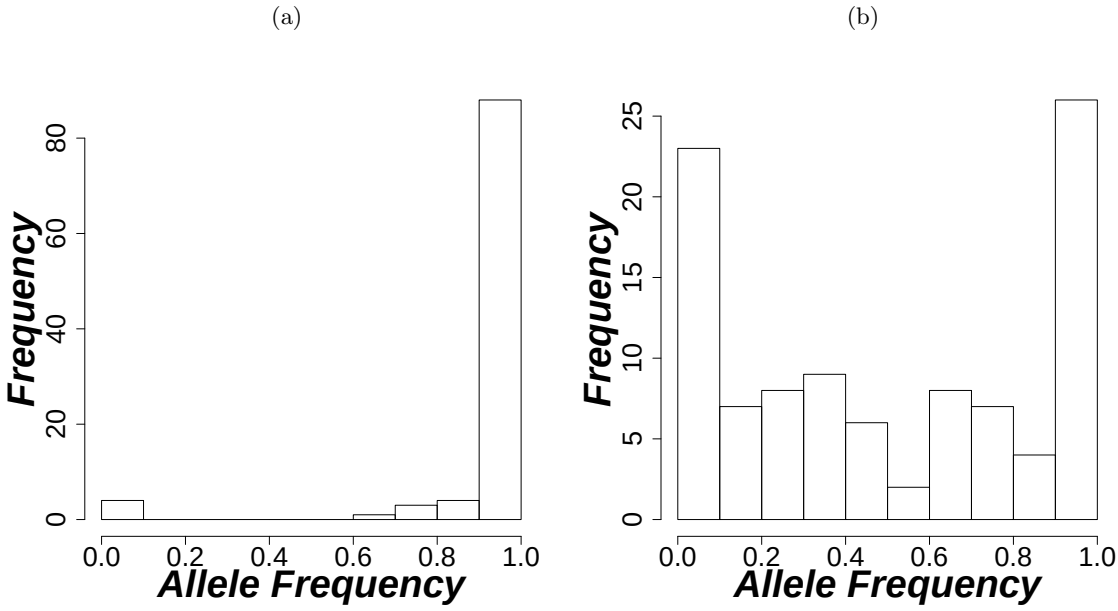

Figure S2.1: Typical examples of the distributions of initial allele frequencies for 100 loci sampled from their respective allele frequency equilibrium distributions determined by population size (N), selection coefficients, mutation rates, and dominance coefficients where applicable (see main text), (a) DM, and (b) HA. In both cases $N = 100$. Other parameters include: For HA, the mean selection coefficient was $\overline{s} = 0.005$ with $s_A = s_a, \mu_a = \mu_A = 0.0005$ while for DM, the mean selection coefficient was $\overline{s} = 0.5$ with $s_A = 0, h = 0.5e^{(-13s_a)}, \mu_A = 0.0005, \mu_a = \mu_A/100$.

S3 Diffusion Approximation and Markov Chain Approaches

S3.1 Diffusion Approximation Approach (DAA)

Here, $f(x,t)$ at a given locus was approximated using the diffusion equation (e.g in Kimura et al. (1955))

$$\frac{\partial f(x,t)}{\partial t} = -\frac{\partial\left[a(x,t)f(x,t)\right]}{\partial x} + \frac{1}{2}\frac{\partial^2\left[b(x,t)f(x,t)\right]}{\partial x^2}, \tag{S3.1}$$

where $a(x,t)$ and $b(x,t)$ refer to the mean and variance of the change in allele frequency during an infinitesimal time interval. For all the mechanisms, we took

$$b(x,t) = \frac{1}{2N_t}x(1-x) \tag{S3.2}$$

(e.g see Durrett (2008)) while $a(x,t)$ depended on the mechanism. For example, assuming s_a and s_A are very small that higher order terms involving s_i^3 and above are negligible, for HA, ID and MA,

$$a(x,t) = x(1-x)\left(s_a(1-x+2hx) - hs_a - s_Ax\right)\left(1 + s_Ax^2 - s_a(1-x)(x-2hx-1)\right) + \mu_a(1-x) - \mu_Ax. \tag{S3.3}$$

The three mechanisms differed in h, s_a and s_A. For FS (see Nabutanyi & Wittmann (2021) supplementary Section A.3),

$$a(x,t) = x(1-x)(x(1-2h_t)+h_t)(1+s_{a,t})(s_a - s_{A,t}) + \mu_a(1-x) - \mu_Ax \tag{S3.4}$$

and for FD,

$$a(x,t) = x(1-x)(s_a(1-x) - s_Ax)(1 + s_Ax^2 + s_a(1-x)^2)/2 + \mu_a(1-x) - \mu_Ax, \tag{S3.5}$$

where, $h_t, h, \mu_a, \mu_A, s_A, s_a, s_{a,t}$, and $s_{A,t}$ are as defined under "Selection Mechanisms" subsection.

We adopted the numerical scheme in Zhao et al. (2013); Xu et al. (2019) to solve Equation (1) subject to the initial condition $f(x,0) = x_0$ and the boundary condition that conserves probability

at all times. The scheme basically discretizes both time t and allele frequency x over the interval 0 and 1 inclusive. The step-length for x is $\frac{1}{m}$, where m is an integer above 0 (used $m = 20$ for all the results) and step-length for time being $\tau > 0$ (in the whole paper, we used $\tau = 1$ so as to correspond to a full generation). The numerical scheme eventually gives a vector of probabilities $f(x_i, t)$ with $i \in \{0, 1, \cdots, m\}$ for each time point as the distribution $f(x, t)$.

S3.2 Markov Chain Approach (MCA)

This approach involved finding the transition probabilities from i copies of a given allele at time t to j copies of the same allele at $t + 1$. Let X be a random variable representing the number of copies of allele A in a population of size N_t at time t. In a diploid population with two alleles at a given locus, there are $2N_t$ alleles in total, and X can take on $\{0, 1, 2, \cdots, 2N_t\}$. The allele copies in the next generation $t + 1$ were randomly sampled (with replacement) from those present at the current generation t. Therefore, X follows a binomial distribution with parameters $2N_t$ and x'' (the allele frequency after selection and mutation acting). Due to computational failure of the binomial distribution for large $N_t > 500$, we approximated the binomial distribution with one of two distributions, the Poisson distribution with parameter $2x''N_{t+1}$ (or $2(1 - x'')N_{t+1}$ when one of the alleles is rare (expected copy number < 35) (Fig. S3.1), and otherwise the normal distribution with parameters $2x''N_{t+1}$ and $2x''(1 - x'')N_{t+1}$ as mean and variance respectively. In summary, the probability of having j allele copies at time $t + 1$ given that i copies are present at time t yields a transition matrix $\mathbf{P}_{ij}$,

$$\mathbf{P}_{ij} = \begin{cases} \mathcal{B}in(j; 2N_{t+1}, x''), & \text{if} \quad N_{t+1} \leq 500, \\ \mathcal{P}oi(j; 2x''N_{t+1}), & \text{if} \;\; N_{t+1} > 500 \;\; \& \;\; 2N_{t+1}x'' < 35, \\ \mathcal{P}oi(2N - j; 2(1 - x'')N_{t+1}), & \text{if} \;\; N_{t+1} > 500 \;\; \& \;\; 2N_{t+1}(1 - x'') < 35, \\ \mathcal{N}(j; 2N_{t+1}, 2x''(1 - x'')N_{t+1}), & \text{elsewhere.} \end{cases} \tag{S3.6}$$

where $\mathcal{B}in(...), \mathcal{P}oi(..)$ and $\mathcal{N}(...)$ are the probability mass functions of the binomial, Poisson and normal distributions respectively. Here, $i = \{0, 1, \cdots, 2N_t\}, j = \{0, 1, \cdots, 2N_{t+1}\}$ and x'' is the frequency of allele A at the end of a given generation t after possible selection and mutation, i.e.,

$x = \frac{i}{2N_t}$, $x' = \frac{x^2 w_{AA} + x(1-x)w_{Aa}}{x^2 w_{AA} + 2x(1-x)w_{Aa} + (1-x)^2 w_{aa}}$ and $x'' = (1-\mu_A)x' + \mu_a(1-x')$. We then normalise each row such that the transition probabilities always sum to 1.

Assuming a population at equilibrium with a constant size N, $\mathbf{P}_{ij}$ is a $(2N+1) \times (2N+1)$ square matrix. The equilibrium distribution of allele copies was obtained by getting the eigenvector corresponding to the largest real part of the eigenvalues (which is always equal to 1) of matrix $\mathbf{P}_{ij}$, which was then normalised to get $f(x,t)$.

S3.2.1 Distribution of Allele Frequencies via Iterating through Generations for the Markov Chain Approach

Similar to the diffusion approximation, the MCA can also be made time-dependent by starting with some initial allele frequency distribution and evaluating the distribution in every generation (Section S3.2.1). Here, the transition matrix is not necessarily a square matrix and allows varying population sizes between generations.

Here, matrix $\mathbf{P}_t$ (subscript t due to change with time) is calculated every generation and is not necessarily a square matrix. $\mathbf{P}$ is generally a $2N_t + 1 \times 2N_{t+1} + 1$ matrix filled according to Equation (S3.6). At each generation $t \geq 0$, the (row vector) distribution of allele copies X is determined as

$$X_{t+1} = X_t \mathbf{P}_t, \tag{S3.7}$$

where we start with some initial allele frequency distribution X_0. The distribution is used in a similar way as in the diffusion approximation to determine population size (Equation (5)). However, this approach is computationally more expensive than the DAA and equilibrium-based MCA.

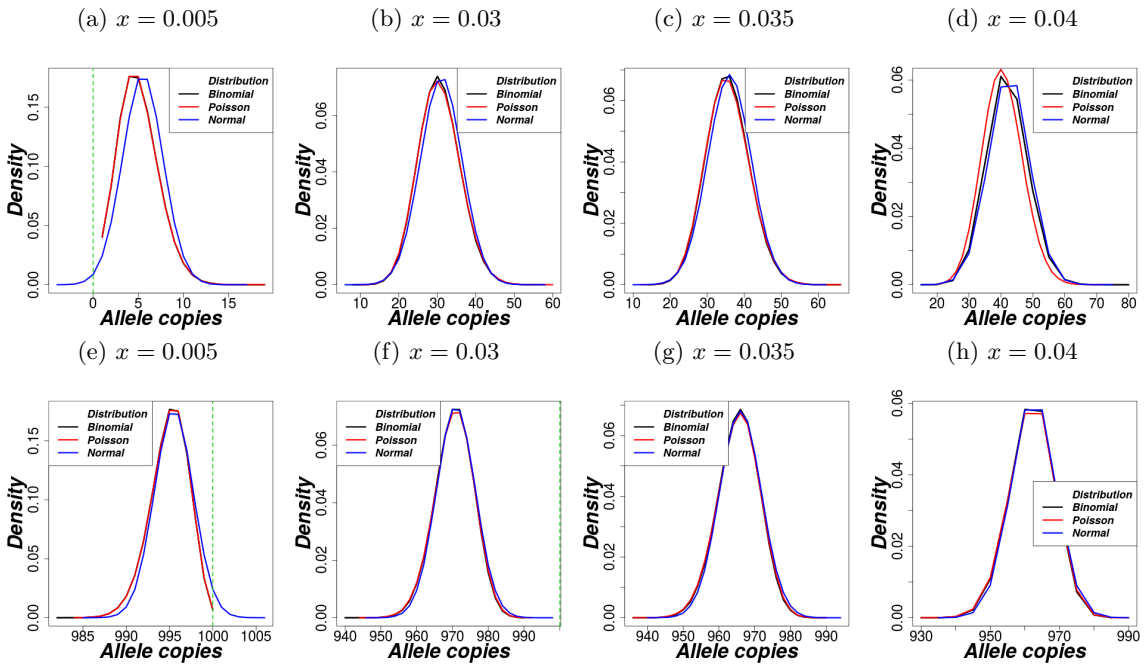

Figure S3.1: Densities for the distribution of allele frequencies with different values of probability, x. The upper panel is obtained from the binomial ($n = 2N, p = x$), Poisson ($\lambda = 2Nx$), and normal ($\mu = 2Nx, \sigma^2 = 2Nx(1-x)$) distributions, while for lower panel, we subtract the random draws (using same parameters) from $2N$; where $N = 500$ and number of draws $= 500000$. The green vertical dotted line is at either 0 or $2N$ to indicate cases where the normal distribution yield non-feasible observations (allele copies below 0 and above $2N$). From these plots, we decided to use the Poisson approximation for less than 35 expected allele copies of the respective rare allele as this threshold yields a good fit to the binomial and avoids negative samples or samples above $2N$ at extreme allele frequencies.

S4 Population trajectories

As mentioned in the main text, DM can model both large-effect and small-effect deleterious mutations. Large-effect deleterious mutations In this section and in the sections after, we present large-effect deleterious mutations via inbreeding depression (ID) and small-effect mutations via mutation accumulation (MA). Therefore, we choose relatively higher values of s_a combined with lower

h for ID, whereas, lower values of s_a and higher h for MA.

S4.1 Population Trajectories from DAA

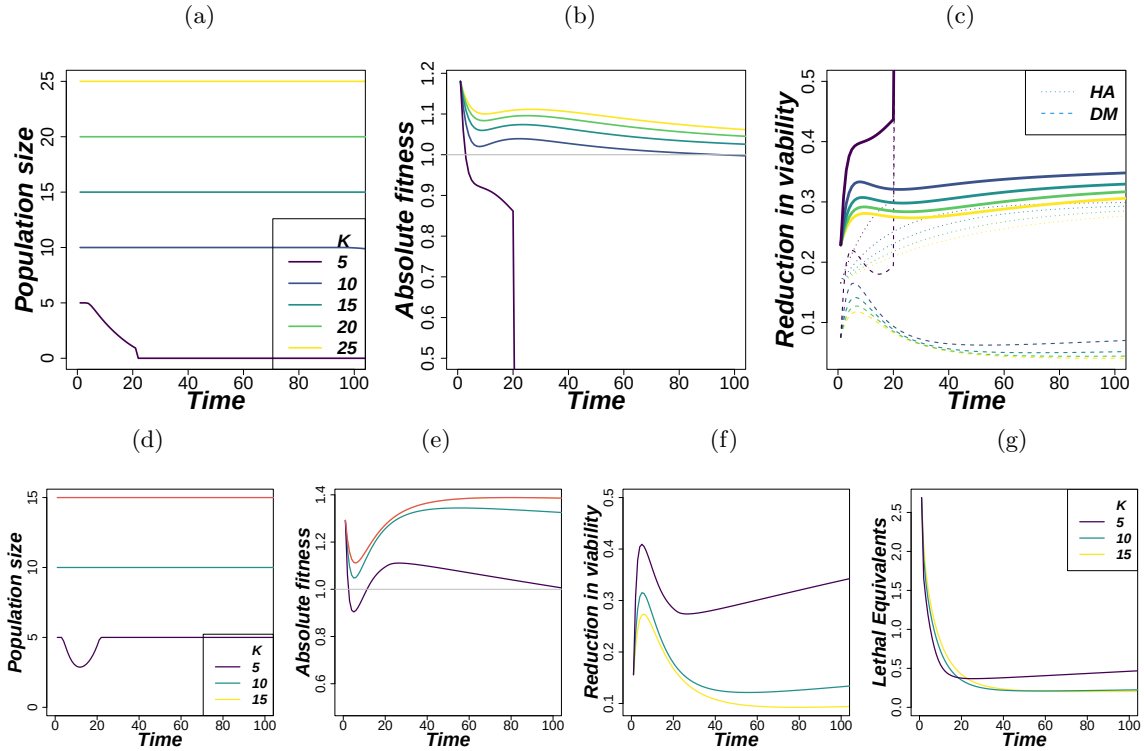

Figure S4.1: Example trajectories zoomed Figure 3. First row: column 1 (for DM) and Second row: column 3 (for HA-DM) in the main text to show the first 100 generations. The thick continuous lines on subfigure (c) is the net reduction in the viability fitness. Subfigure (g) shows how number of lethal equivalents for DM. Parameters were as described in Table 1 in the main text. Other shared parameters are $n = 100$. 50 loci were under each mechanism for the 1st row.

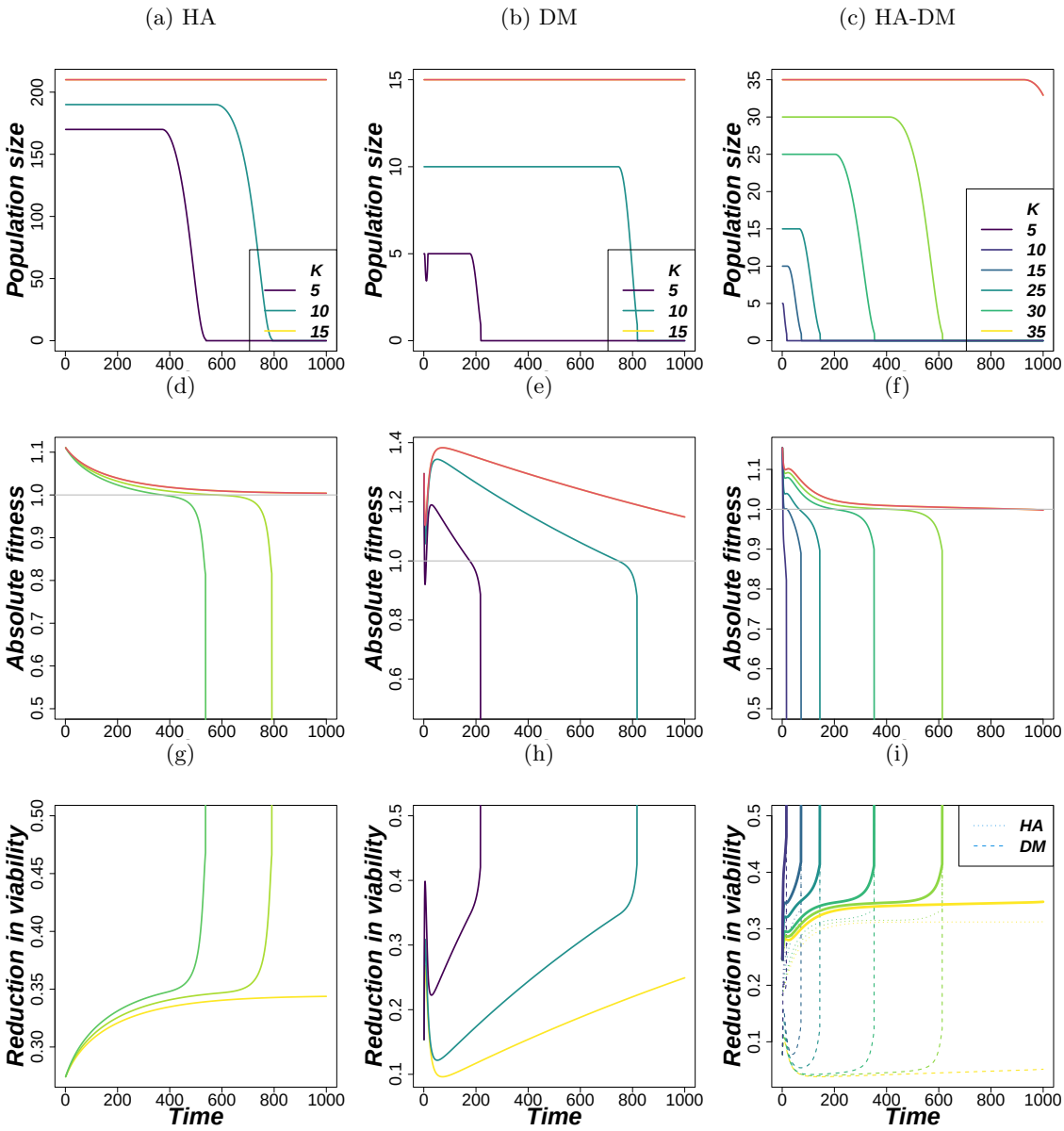

Figure S4.2: Example of typical trajectories under various carrying capacities with selection coefficients sampled from a distribution. The initial allele frequency for HA was 0.5 across all loci while that for DM was calculated from the deterministic equilibrium frequency (i.e., deleterious allele a with $x_0 = \sqrt{\frac{\mu_A}{s_a}}$ when $\frac{s_a}{h} \geq 1$, otherwise $x_0 = \frac{\mu_A}{h \times s_a}$). Column 1: HA, Column 2: DM, and Column 3: HA-DM, while for Row 1: population size, Row 2: absolute fitness, Row 3: reduction in viability fitness. The trajectories were obtained using the diffusion approximation approach The gray horizontal line is the threshold absolute fitness of 1 while the red lines indicate the MVP size. The thick continuous lines on subfigure (i) is the net reduction in the viability fitness. Selection parameters were as described in Table 1 and Section S2 Other shared parameters were $n = 100$. For scenarios with two selection mechanisms (column 3), 50 loci were under each mechanism.

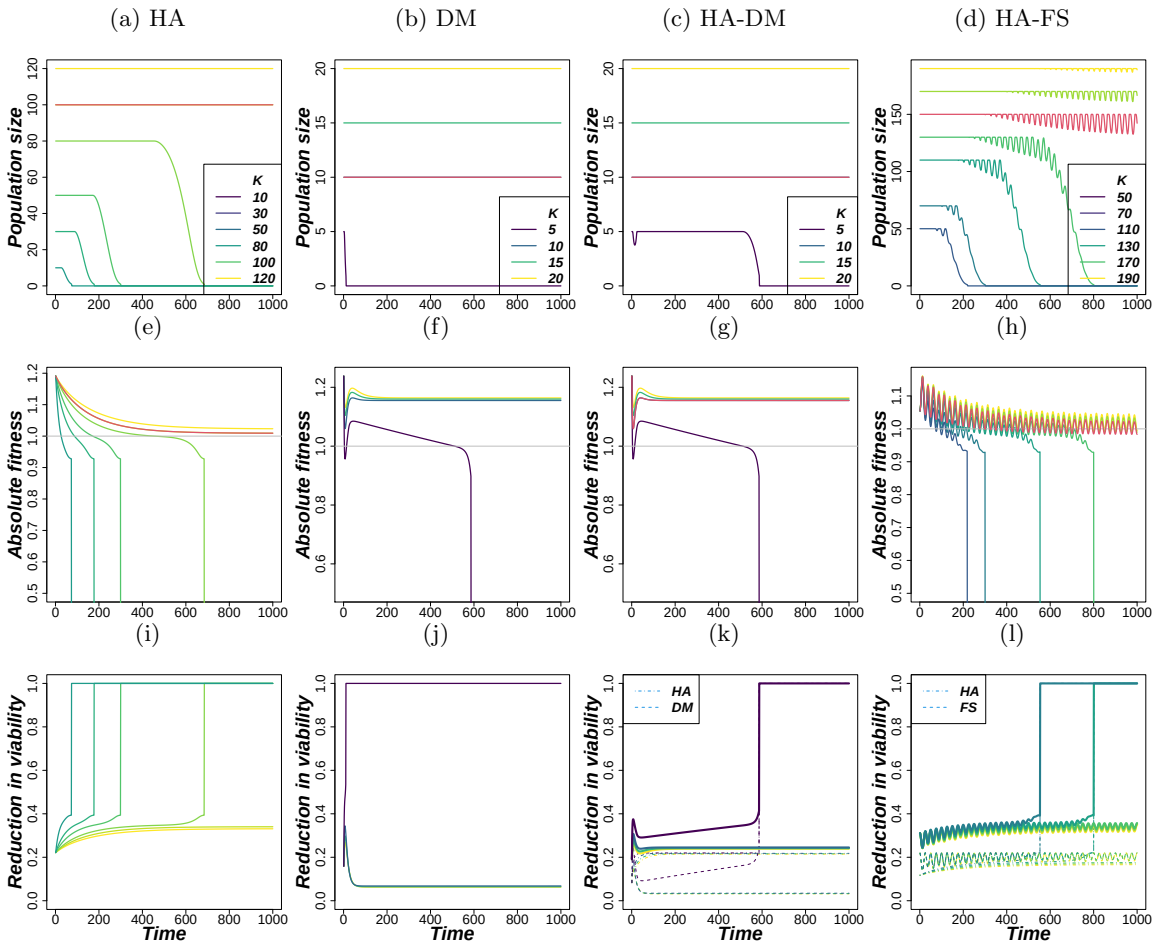

Figure S4.3:

Example trajectories under various carrying capacities with uniform selection coefficients and initial allele frequencies across loci for; Column 1: HA, Column 2: DM, Column 3: HA-DM and Column 4: HA-FS while for Row 1: population size, Row 2: absolute fitness and Row 3: reduction in offspring viability fitness for each constituent mechanism. The thick continuous lines on subfigures (k) and (l) is the net reduction in the viability fitness. The trajectories were obtained using the diffusion approximation approach. The gray horizontal line is the threshold absolute fitness of 1 while the red lines indicated the recorded MVP size. For balancing selection, $s_a = s_A = 0.005, \mu_A = \mu_a = 0.0005$ and for DM $s_A = 0, s_a = 0.5, h = 0.01, \mu_A = 0.0005, \mu_a = \frac{\mu_A}{100}$. Other shared parameters are $n = 100, K = N_0, r = \ln(1.53)$. For scenarios with two selection mechanisms (columns 3 and 4), 50 loci were under each mechanism.

S4.1.1 Longer-time trajectories

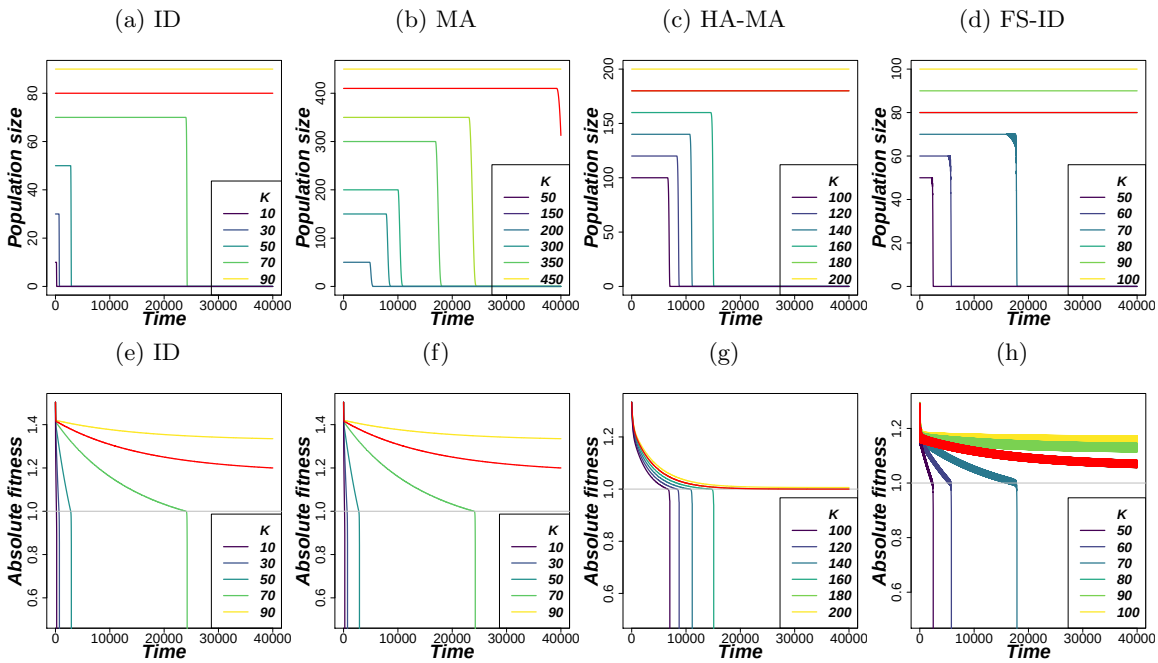

Figure S4.4: Longer-time population and fitness trajectories (run for 40000 generations) for various carrying capacities using the diffusion approximation approach. The gray horizontal line is the threshold absolute fitness of 1. The red line shows the MVP size estimate. In cases of more than one selection mechanism, the number of loci under each mechanism was equal. ID and MA are the different forms of DM, differing in magnitude of s_a and h. Parameters for balancing selection were $s_a = s_A = 0.005, \mu_A = \mu_a = 0.0005, \kappa = 50$ and for DM $s_A = 0, \mu_A = 0.0005, \mu_a = \frac{\mu_A}{100}$, for ID, $s_a = 0.05, h = 0.01$, and MA, $s_a = 0.005, h = 0.5$. Other shared parameters were $n = 100, K = N_0, r = \ln(1.53)$.

S4.2 Population Trajectories from the IBM

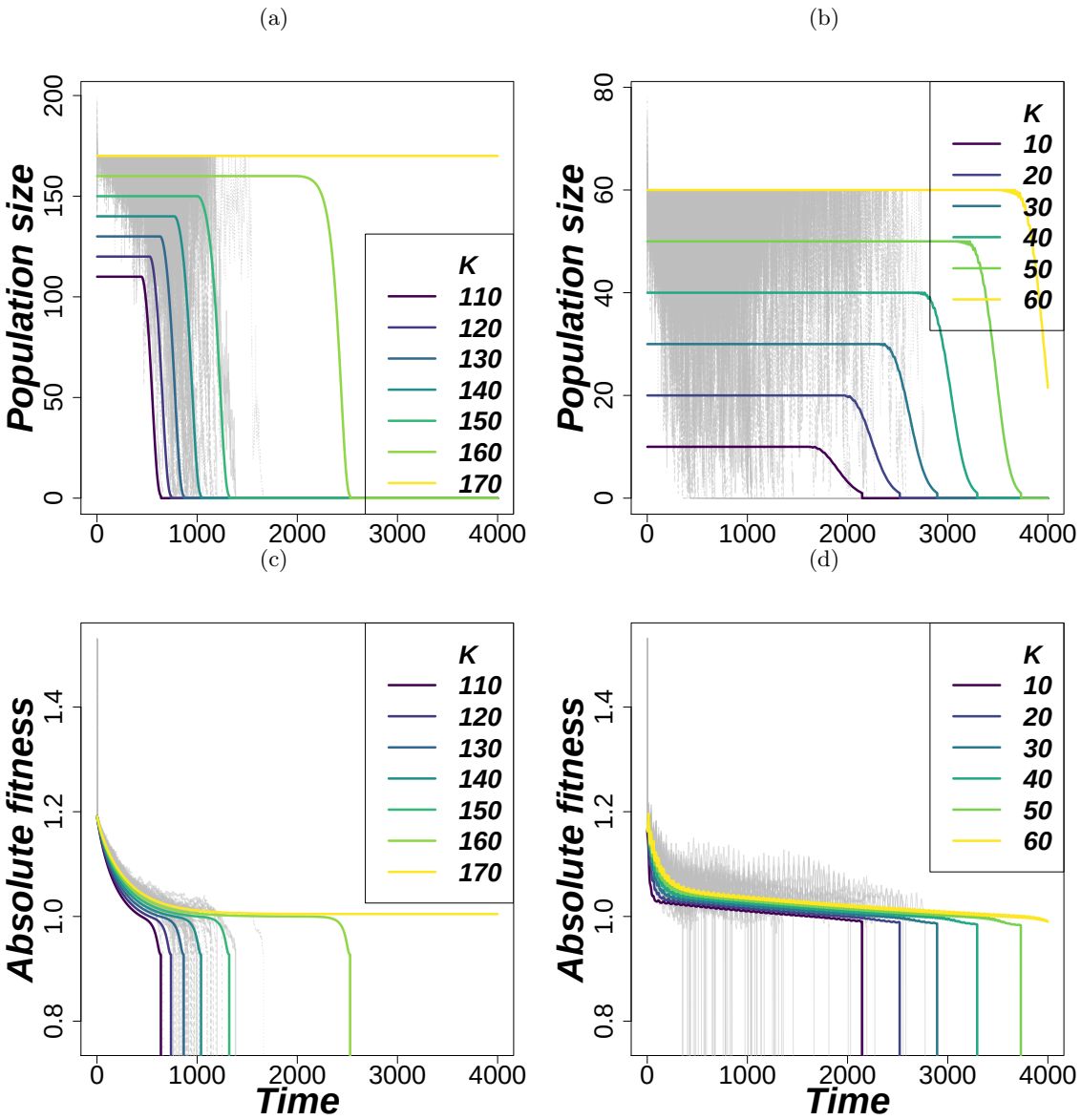

Figure S4.5: Individual-based simulations of 60 trajectories (in gray) for HA at $K = 170$ (column 1) and HA-FS-FD-ID-MA at $K = 60$ (column 2). Here DM is represented twice by ID and MA where ID has more deleterious alleles than MA. The selection coefficients are uniform across loci under a given selection mechanism. The thick lines are for various carrying capacities using the diffusion approximation approach. Parameters for balancing selection are $s_a = s_A = 0.005, \mu_A = \mu_a = 0.00022, \kappa = 50$. For MA, $s_A = 0, s_a = 0.005, \mu_A = 0.00022, \mu_a = \frac{\mu_A}{100}$ with $h = 0.5$ for MA and $h = 0.0$ for ID. Other shared parameters were $n = 100$. In column 2, the number of loci under each mechanism was equal (i.e., 20 loci each).

S5 Critical Number of Loci and Equilibrium Fitness

S5.1 Equilibrium Fitness

We start with single-locus dynamics where the mean fitness is obtained from the deterministic equilibrium allele frequency x (which would be reached in a population of infinite size) as

$$\overline{w}(x) = x^2 w_{AA} + 2x(1-x)w_{Aa} + (1-x)w_{aa}, \tag{S5.1}$$

where $w_{ij}, \quad i,j \in \{A,a\}$ is the genotype fitness (geometric mean fitness in a complete cycle for FS) and $\overline{w}$ is the mean locus fitness for a given mechanism. Assuming equilibrium conditions and for symmetric selection, the equilibrium mean fitness for HA is given by

$$\overline{w} = 1 - \frac{s}{2}, \tag{S5.2}$$

where s is the selection coefficient against homozygotes.

For a purely recessive deleterious allele, the fitness is given by (assuming Hardy-Weinberg proportions in an infinite population; Felsenstein (2015))

$$\overline{w} = 1 - (1-\overline{x})s_a, \tag{S5.3}$$

where s_a the selection coefficients against the homozygote of the recessive allele a and $\overline{x}$ is the equilibrium frequency of wild-type allele A approximated by

$$\overline{x} = 1 - \sqrt{\frac{\mu_A}{s_a}}. \tag{S5.4}$$

However, when the deleterious allele is not completely recessive,

$$\overline{w} = 1 - 2\overline{x}(1-\overline{x})hs_a - (1-\overline{x})^2 s_a, \tag{S5.5}$$

where $h > 0$ is the dominance coefficient and this time $\overline{x}$ is approximated by

$$\overline{x} = 1 - \frac{\mu_A}{hs_a}. \tag{S5.6}$$

Note that when $s_a < \mu_A$ in Equation S5.4 and $hs_a < \mu_A$ in Equation S5.6 gives $\overline{w} > 1$ which does not make sense. So, the approximations fail for these cases because the equilibrium allele frequency of the wild-type allele will be below 0. Ideally, in such cases, selection against deleterious allele is so weak and yet their inflow via mutation is so high and thus it will result into fixation of the deleterious allele.

In Fig. S5.1, we show effect of increasing selection coefficient and mutation rates on MVP estimates for loci under mutation-selection-drift equilibrium. At a given mutation rate, as s_a (or hs_a) increases, the MVP size decreases. Also, for a given selection coefficient, increase in mutation rate increases MVP size estimates. These observations are expected as shown from Equations (S5.4) and (S5.6). The increase in s_a reduces the frequency of the deleterious allele. Thus strong purging of deleterious alleles eventually leads to a higher equilibrium fitness. On the other hand, increase in μ_A increases frequency of the deleterious mutation at equilibrium leading to low equilibrium fitness.

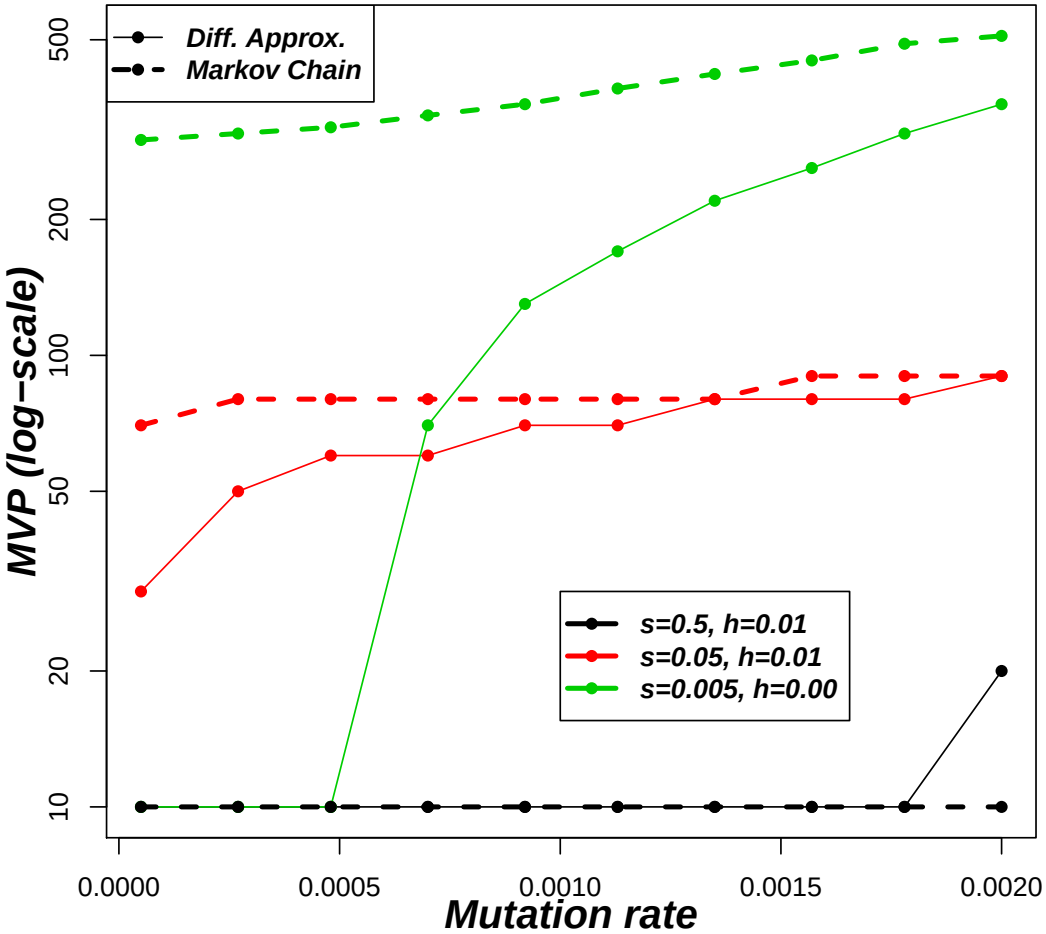

Figure S5.1: MVP estimates for populations under different selection pressure from DM with fixed number of loci $n = 100$ and $s_A = 0$. The indicated values in the legend are for s_a. On the x-axis, we have the forward mutation rate μ_A. Other parameters are $\mu_a = \frac{\mu_A}{100}, Tmax = 4000$.

S5.2 Critical number of loci

There can be a critical number of loci n_c, above which no arbitrary size of a population can survive. Here, n_c is obtained based on the assumption that absolute fitness of 1 is the threshold below which

populations go extinct i.e., $\overline{V}^n E < 1$, where n is the number of loci under selection and E is the expected number of offspring per individual:

$$n_c = \frac{-\ln(E)}{\ln(\overline{V})}. \tag{S5.7}$$

We illustrate how n_c varies with selection coefficient, fitness and mutation rate in Figure S5.2.

For two mechanisms, we can compute the maximum number of additional loci n_{1c} under mechanism 1 with equilibrium mean fitness per locus V_1 that can still allow finite-sized populations to survive when there are already n_0 loci under mechanism 0 with equilibrium mean fitness per locus V_0. We have $\overline{V}_1^{n_{1c}} \overline{V}_0^{n_0} E = 1$ and

$$n_{1c} = \frac{\ln(\frac{1}{(\overline{V}_0^{n_0} \cdot E)})}{\ln \overline{V}_1} = -\frac{n_0 \ln(\overline{V}_0) + \ln(E)}{\ln \overline{V}_1}. \tag{S5.8}$$

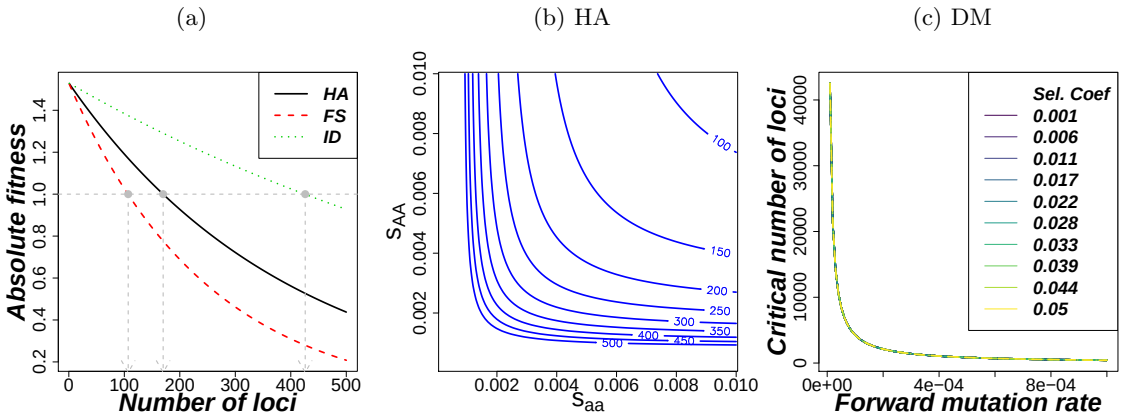

Figure S5.2: (a) How absolute fitness changes with increasing number of loci under selection (assuming infinite population size). Parameters used $s_a = s_A = 0.005$ for HA and FS, $s_a = 0.05, s_A = 0, \mu = 0.001, h = 0$ for DM (here indicated as ID) (b) Shows how critical number of loci (that results into an asymptotic increase in MVPs) varies with selection coefficients in HA (from Equation (S5.7)). (c) Shows how the critical number of loci under selection varies with mutation rate μ_A for different selection coefficients for DM. Parameters used $h = 0, \overline{x} = \sqrt{\mu_A / s_a}$ for the deleterious allele.

S5.3 Effect of Number of Loci on MVP estimates from the MCA

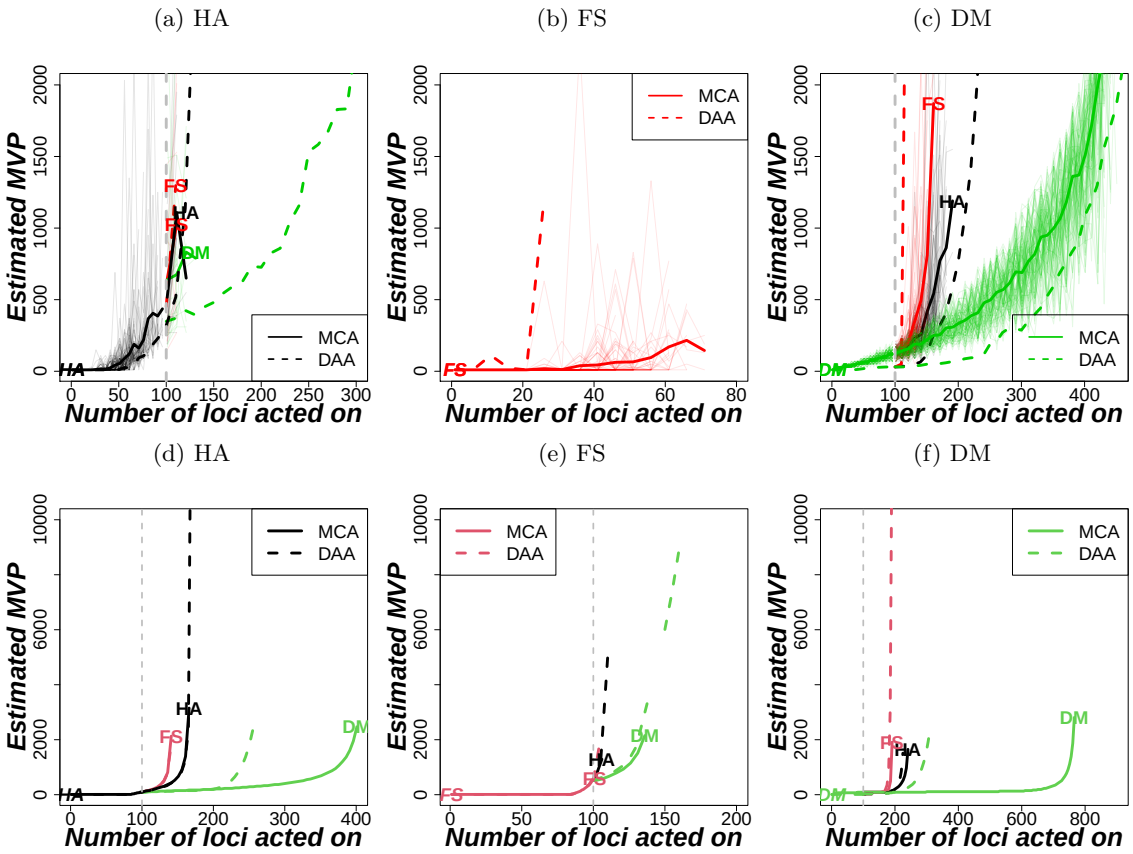

Figure S5.3: Effect of increasing number of loci under selection on MVP size. Same data as in 4 but the y-axis not log-scaled and limited to a maximum of 2000 for Row 1 and 10000 for Row 2.

S6 MVP Estimates from Fixed Number of Loci

S6.1 MVP Estimates from IBM with Fixed Number of Loci

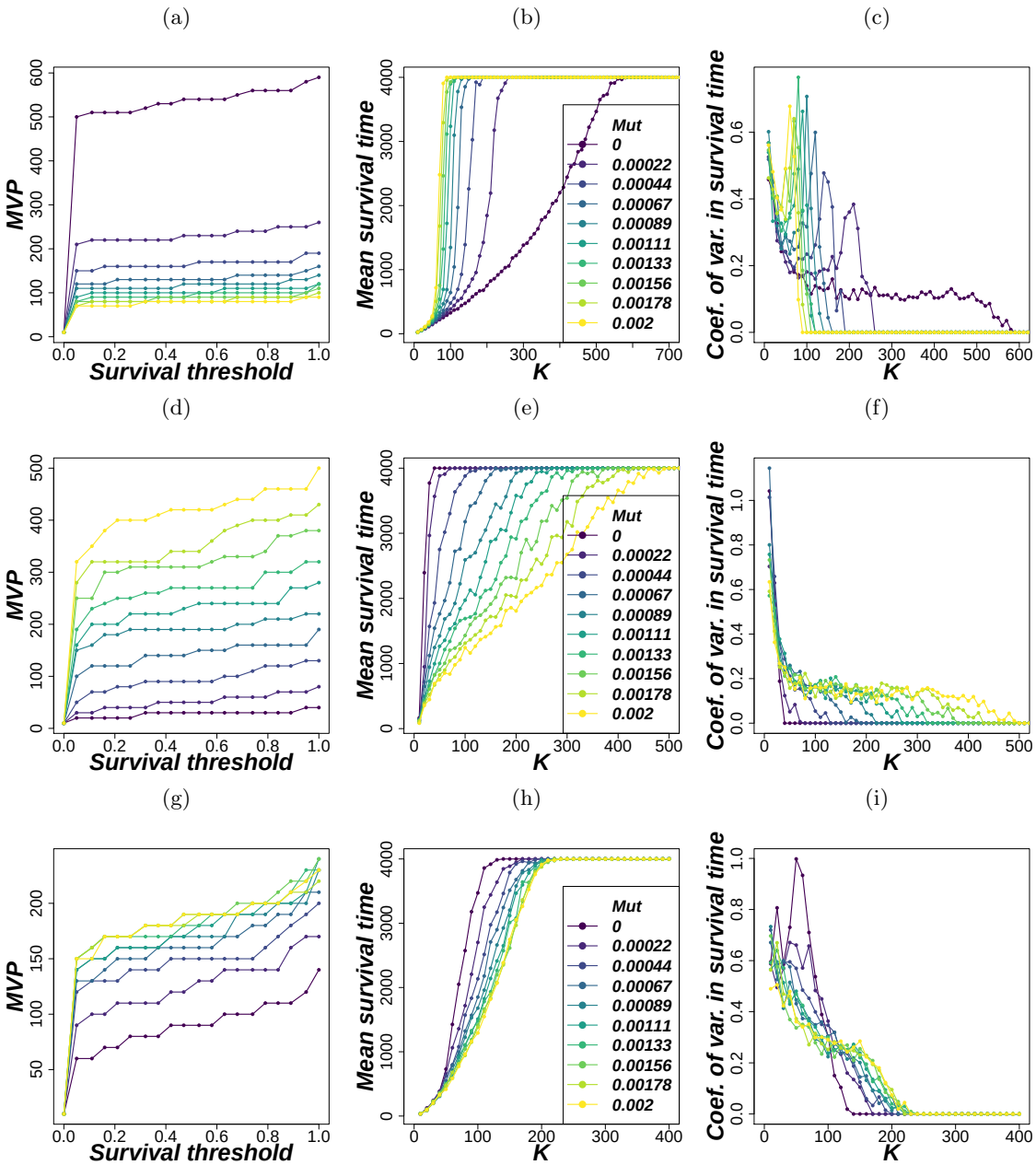

Figure S6.1: MVP estimates from the IBM with uniform selection coefficients across loci. Row 1: HA only, Row 2: DM only, and Row 3: HA-FS-FD-ID-MA (ID and MA represent DM with different values of s_a and h). 1st column: MVP estimates for different mutation rates measured at different levels of survival probability. 2nd column: Mean survival time of populations at different carrying capacities estimated under different mutation rates. 3rd column: Coefficient of variation in survival times of populations at different carrying capacities estimated under different mutation rates. Parameters for balancing selection; $s_a = s_A = 0.005, \mu_A = \mu_a, \kappa = 50$, for ID and MA $s_A = 0, s_a = 0.005, \mu_a = \frac{\mu_A}{100}$ while $h = 0.5$ for MA and $h = 0$ for ID. Other shared parameters were $K = N_0, r = \ln(1.53)$ and a total of 100 loci were equally shared by the constituent mechanisms.

Figure S6.1 shows MVP size estimates from the IBM. The MVP size estimates from the IBM were qualitatively similar to those estimated by DAA and MCA (Fig. 5 in the main text). Quantitatively, estimates from the IBM were (slightly) higher than corresponding estimates (Fig. 5 row 2). The MVP estimates were fairly insensitive to levels of survival probability threshold (Fig. S6.1 column 1). As expected, the mean time to extinction increased rapidly with increasing carrying capacity K (Fig. S6.1 column 2) Also, there was more uncertainty in the extinction times in populations with lower carrying capacities than their counterparts with large capacities (Fig. S6.1 column 3).

S6.2 MVP Estimates with Fixed Number of Loci Including those from Negative Frequency-Dependent Selection (FD)

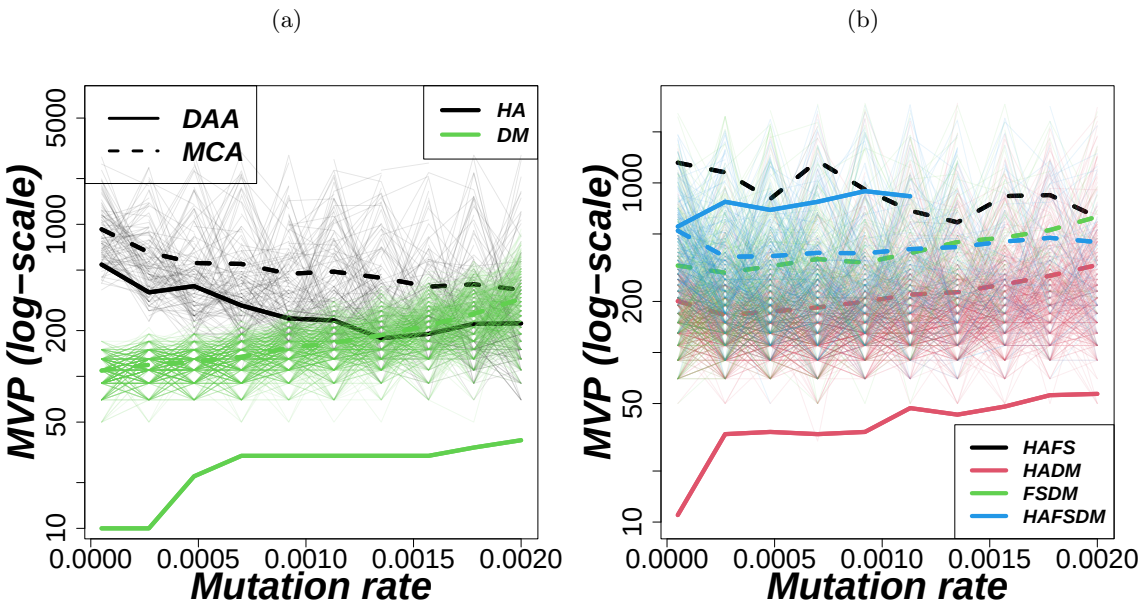

Figure S6.2: Same parameters as in Figure 5, 1st row; in the main text only that the initial allele frequency across loci is uniform for a given selection mechanism. That is, 0.5 for balancing selection mechanisms and 0.95 for DM.

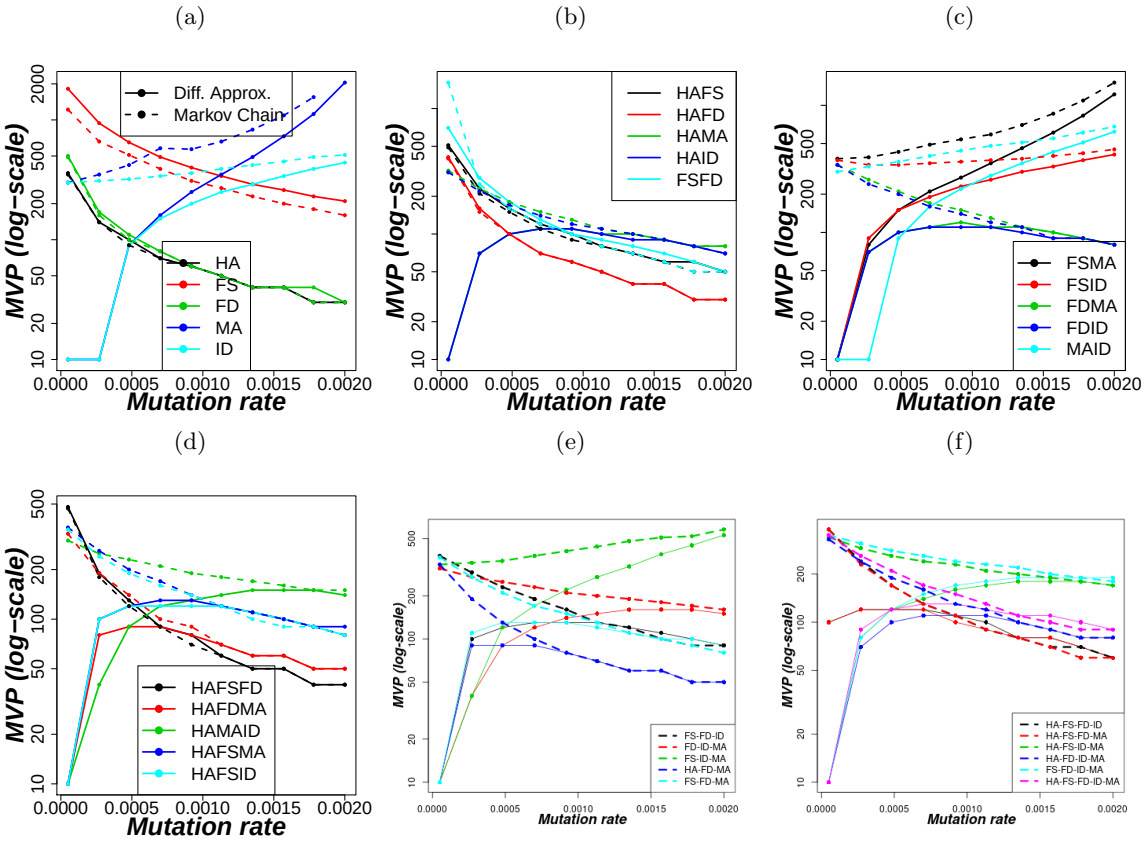

Figure S6.3: MVP estimates from the Markov chain approach (with broken thick lines) and the diffusion approximation (with unbroken thin lines) under uniform selection coefficients across loci with $T_{max} = 4000$. ID and MA represent DM with different s_a and h values. Parameters $s_a = s_A = 0.005, K = N_0, r = \ln(1.53), \mu_A = \mu_a, \kappa = 50$ except for ID and MA where $s_A = 0, \mu_a = \frac{\mu_A}{100}$ and also for ID, $h = 0.5$. The total number of loci on the genome is $n = 100$ except for genomes with 3 selection mechanisms where $n = 99$ for purposes of equal distribution of loci.

S6.3 Arithmetic, Geometric and Harmonic Mean of the MVPs from Constituent Selection Mechanisms

(a) DAA (b) MCA

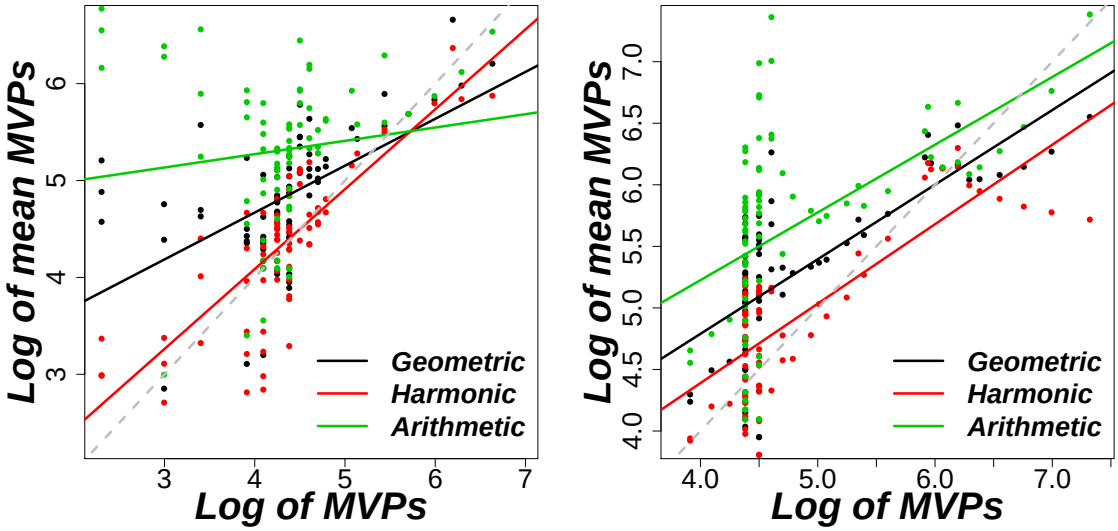

Figure S6.4: Comparison of the estimated MVPs (on x axis) to the geometric, harmonic and arithmetic means (on y axis) of the constituent isolated selection mechanisms for a given scenario using (a) the diffusion approximation and (b) the Markov chain approaches. The different colours show different calculated means (black, red, and green points for geometric, harmonic, and arithmetic means respectively) while the solid lines are the regression lines for each calculated mean. Parameters were as in Fig. S6.3. The points are from HAFS, HAID, FSMA, MAID, HAFSMA, HAFSID, FSMAID, and HAFSMAID.

In Fig. S6.4, we compare the joint MVP to the different means of the MVPs estimated from the isolated selection mechanisms. Generally, the observed MVPs under a mixture of mechanisms are closer to the harmonic and geometric means than the arithmetic mean of the MVPs calculated for the mechanisms in isolation with the same total number of loci. To a large extent, the joint MVPs are (slightly) above the calculated harmonic means and (slightly) below the geometric means. We briefly illustrate why joint MVP is closer to the harmonic mean in Section S7.

S7 Relationship between MVP estimates and fitness across loci

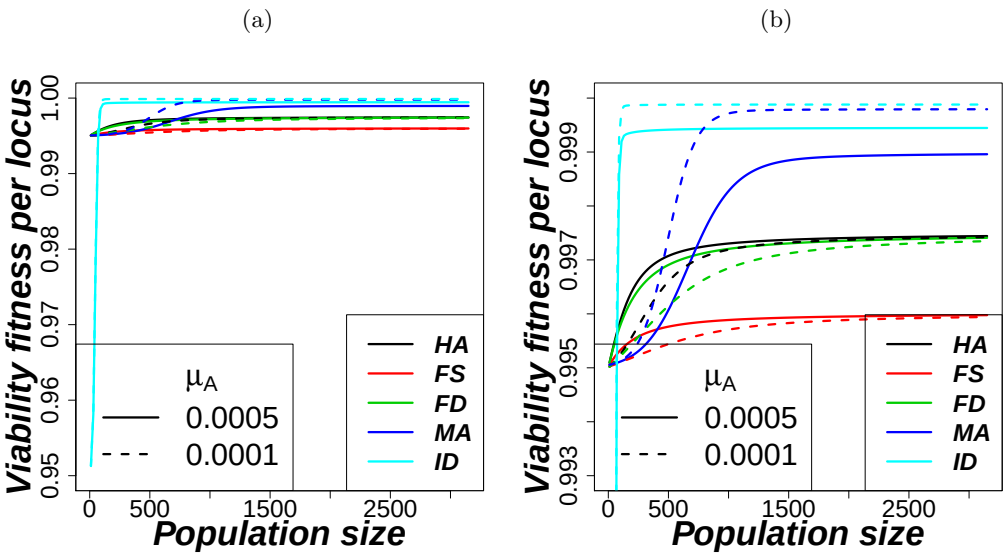

Figure S7.1: Viability fitness per locus at different population sizes for the different mechanisms from the Markov chain approach at equilibrium (Equation (S3.6)). Parameters: $s_a = s_A = 0.005, \mu_A = \mu_a, \kappa = 50$ for balancing selection mechanisms and for MA: $s_A = 0, s_a = 0.005, h = 0.5, \mu_a = \frac{\mu_A}{100}$, and ID: $s_A = 0, s_a = 0.05, h = 0.01, \mu_a = \frac{\mu_A}{100}$. Panel (b) zooms in on the upper viability range in (a).

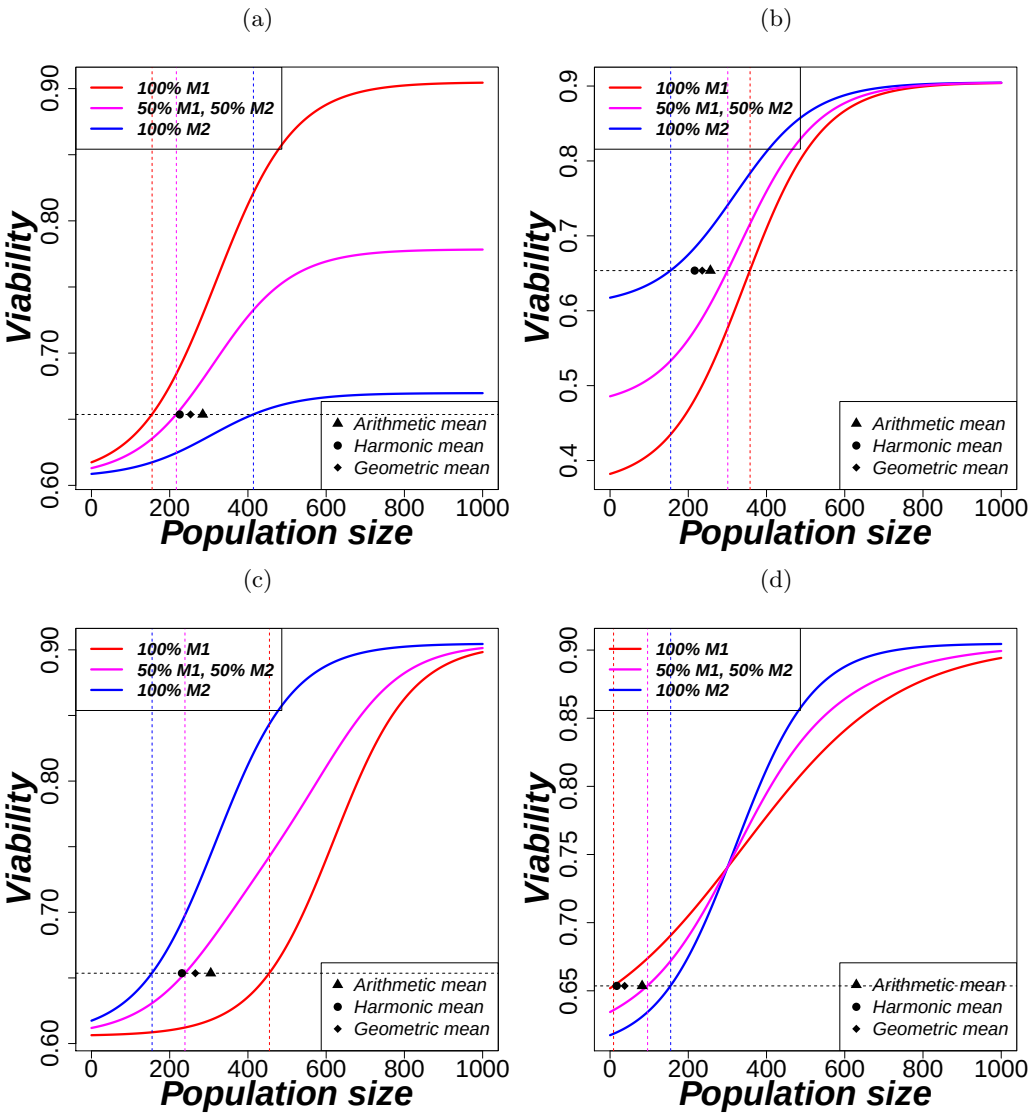

Figure S7.2: Logistic curve fitting $V = V_{min} + \frac{V_{max}-V_{min}}{1+e^{-m(N-N_m)}}$, where V is the viability per locus, V_{min} and V_{max} are the minimum and maximum viability per locus, and N_m is the population size N of the viability sigmoid midpoint, and m is steepness of the curve. Illustration of the relationship between minimum viable population sizes in a logistic curve setting (as observed from Figure S7.1). To get viability for a single mechanism with $n = 100$ loci, we simple use V^n (blue and red solid lines), and for two mechanisms, we use $V_1^{n/2} \times V_2^{n/2}$ (magenta solid line). The corresponding minimum viable population sizes with a critical viability $v_{crit} = 1/E = 1/1.53$ are shown as dashed vertical lines. The circle, diamond, and triangle indicate the harmonic, geometric, and arithmetic mean of the two separate minimum viable population sizes, respectively.

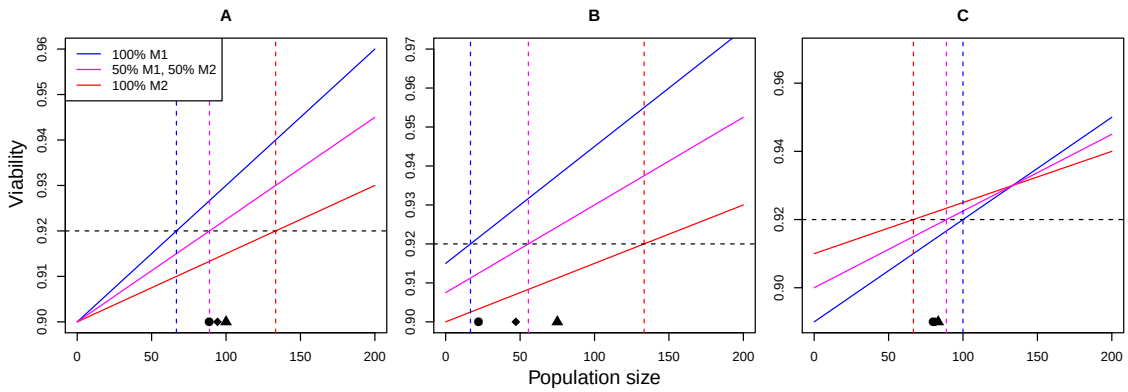

Figure S7.3: Illustration of the relationship between minimum viable population sizes in a simple linear setting. Assuming approximately additive effects of small fitness reductions, the viability with 50% of loci under mechanism 1 and 50% under mechanism 2 for a given population size (magenta solid line) is the arithmetic mean of viabilities for the two separate mechanisms acting at 100% of loci (blue and red solid lines). The corresponding minimum viable population sizes with a critical viability $v_{crit} = 1/E = 0.92$ are shown as dashed vertical lines. The circle, diamond, and triangle indicate the harmonic, geometric, and arithmetic mean of the two separate minimum viable population sizes, respectively.

Here we use a simple setting to illustrate possible relationships between MVP sizes under single versus multiple genetic mechanisms. For this section, we assume that the relationship between population size and viability at low population sizes can be well approximated by a linear relationship (Figures S7.1 and S7.2). Assume that we have two genetic mechanisms ($i = 1, 2$) that when acting at n loci have viability

$$V = v_{min,i} + m_i \cdot N. \tag{S7.1}$$

The respective minimum viable population size then is the population size at which viability takes the critical value $v_{crit} = 1/E$ at which absolute fitness is 1. Thus,

$$v_{crit} = v_{min,i} + m_i \cdot MVP_i \tag{S7.2}$$

$$\Leftrightarrow MVP = \frac{v_{crit} - v_{min,i}}{m_i}. \tag{S7.3}$$

As long as deviations of viability from 1 are small, loci make roughly additive contributions to reducing viability and thus the viability relationship with half of the loci under mechanisms 1 and half of the loci under mechanism 2 is

$$V = \frac{v_{min,1} + v_{min,2}}{2} + \frac{m_1 + m_2}{2} \cdot N \tag{S7.4}$$

and the corresponding minimum viable population size is

$$MVP_{joint} = \frac{v_{crit} - \frac{v_{min,1}+v_{min,2}}{2}}{\frac{m_1+m_2}{2}} = \frac{C_1 + C_2}{\frac{C_1}{MVP_1} + \frac{C_2}{MVP_2}}, \tag{S7.5}$$

where $C_i = v_{crit} - v_{min,i}, \quad i = 1, 2.$

We now consider three different exemplary cases (Fig. S7.3). In the first case (Fig. S7.3 A), the two mechanisms have the same minimum viability $v_{min,1} = v_{min,2} = v_{min}$ (i.e., $C_1 = C_2$) as was also approximately the case in Fig. S7.1. Then

$$MVP_{joint} = \frac{v_{crit} - v_{min}}{\frac{m_1+m_2}{2}} = \frac{1}{\frac{1}{2} \cdot \frac{m_1}{v_{crit}-v_{min}} + \frac{m_2}{v_{crit}-v_{min}}} = \frac{2}{\frac{1}{MVP_1} + \frac{1}{MVP_2}}. \tag{S7.6}$$

That is, the joint minimum viable population size (magenta vertical line in Fig. S7.3 A) is equal to the harmonic mean (indicated by a black dot in Fig. S7.3 A) of MVP sizes under mechanism 1 and 2. Intuitively, this is the case because minimum viable population size is inversely proportional to the rate at which viability increases with increasing population size. This is approximately true even when the viability functions are nonlinear and thus explains why we often obtain joint MVP sizes close to the harmonic mean of individual MVP sizes.

However, this equality does not hold if the two mechanisms have different v_{min} (i.e., $C_1 \neq C_2$). Depending on the relation of the two slopes and intercepts, we can then get scenarios where the joint MVP is larger than the harmonic mean of MVPs but still smaller than the arithmetic mean (Fig. S7.3 B) or scenarios where the joint MVP is even larger than the arithmetic mean of MVPs (Fig. S7.3 C). Also for general nonlinear viability functions, all cases are possible and the exact relationship between MVPs will depend on the precise shape of the curves.

S8 Initial allele frequency

Figure S8.1 shows how initial allele frequency affects MVP estimates at different mutation rates for different isolated mechanisms. Initial allele frequency has large effects in FS. For loci under mutation-selection-drift balance (ID and MA), MVPs are insensitive to initial allele frequency unless the frequency of the deleterious allele is extreme, e.g. above 90%. Similarly, for HA, only very extreme allele frequencies have an effect on MVP sizes.

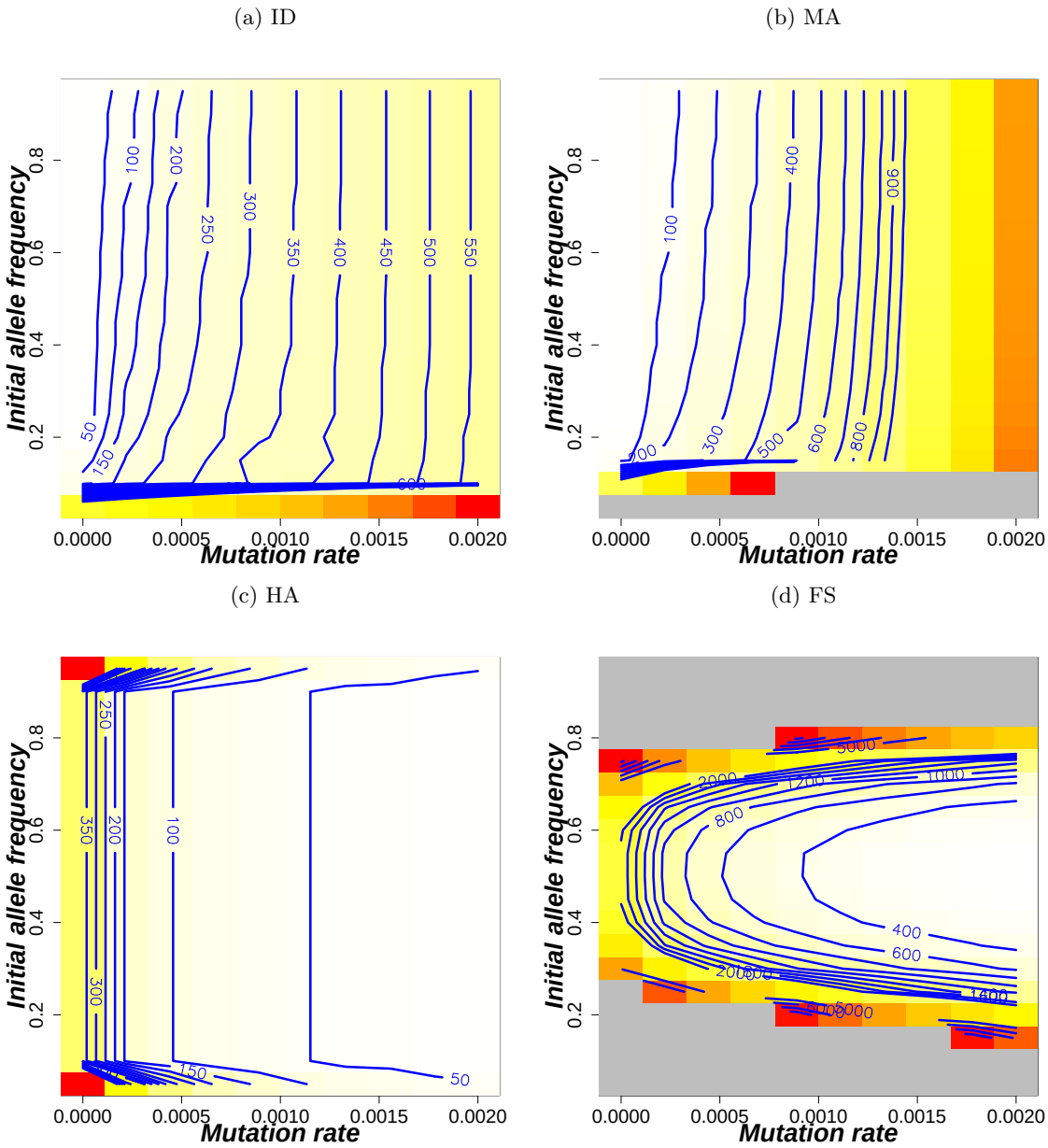

Figure S8.1: Effect of initial allele frequency on MVP size estimates. The blue lines show MVP trajectories at given initial allele frequency. The parameters for balancing selection were $s_a = s_A = 0.005, \mu_A = \mu_a, \kappa = 50$, for ID and MA $s_A = 0, s_a = 0.005, \mu_a = \frac{\mu_A}{100}$ while $h = 0.5$ and $h = 0$ were respectively for MA and ID. Other shared parameters were $K = N_0, r = \ln(1.53)$. The gray shaded parts have their MVP estimates above 10000.